Accepted Manuscript

Contrasting styles of post-caldera volcanism along the Main Ethiopian Rift: Implications for contemporary volcanic hazards

Karen Fontijn, Keri McNamara, Amdemichael Zafu Tadesse, David M. Pyle, Firawalin Dessalegn, William Hutchison, Tamsin A. Mather, Gezahegn Yirgu

Please cite this article as: Karen Fontijn, Keri McNamara, Amdemichael Zafu Tadesse, David M. Pyle, Firawalin Dessalegn, William Hutchison, Tamsin A. Mather, Gezahegn Yirgu , Contrasting styles of post-caldera volcanism along the Main Ethiopian Rift: Implications for contemporary volcanic hazards. The address for the corresponding author was captured as affiliation for all authors. Please check if appropriate. Volgeo(2017), https://doi.org/10.1016/j.jvolgeores.2018.02.001

Contrasting styles of post-caldera volcanism along the Main Ethiopian Rift: Implications for contemporary volcanic hazards

Karen Fontijn[1,*], Keri McNamara[2], Amdemichael Zafu Tadesse[3], David M Pyle[1], Firawalin Dessalegn[4], William Hutchison[5], Tamsin A Mather[1], Gezahegn Yirgu[3]

[1]Department of Earth Sciences, University of Oxford, United Kingdom

[2]School of Earth Sciences, University of Bristol, United Kingdom

[3]School of Earth Sciences, Addis Ababa University, Ethiopia

[4] Department of Geology, Wollega University, Ethiopia

[5] School of Earth and Environmental Sciences, University of St. Andrews, United Kingdom

*Corresponding author: Karen.Fontijn@earth.ox.ac.uk, karen.fontijn@gmail.com, Tel +44 1865 272045

Abstract

The Main Ethiopian Rift (MER, ~7-9 °N) is the type example of a magma-assisted continental rift. The rift axis is populated with regularly spaced silicic caldera complexes and central stratovolcanoes, interspersed with large fields of small mafic scoria cones. The recent (latest Pleistocene to Holocene) history of volcanism in the MER is poorly known, and no eruptions have occurred in the living memory of the local population. Assessment of contemporary

volcanic hazards and associated risk is primarily based on the study of the most recent eruptive products, typically those emplaced within the last 10-20 ky. We integrate new and published field observations and geochemical data on tephra deposits from the main Late Quaternary volcanic centres in the central MER to assess contemporary volcanic hazards.

Most central volcanoes in the MER host large mid-Pleistocene calderas, with typical diameters of 5-15 km, and associated ignimbrites of trachyte and peralkaline rhyolite composition. In contrast, post-caldera activity at most centres comprises eruptions of peralkaline rhyolitic magmas as obsidian flows, domes and pumice cones. The frequency and magnitude of events varies between individual volcanoes. Some volcanoes have predominantly erupted obsidian lava flows in their most recent post-caldera stage (Fentale), whereas other have had up to 3 moderate-scale (VEI 3-4) explosive eruptions per millennium (Aluto). At some volcanoes we find evidence for multiple large explosive eruptions (Corbetti, Bora-Baricha, Boset-Bericha) which have deposited several centimetres to metres of pumice and ash in currently densely populated regions. This new overview has important implications when assessing the present-day volcanic hazard in this rapidly developing region.

Key words

Main Ethiopian Rift; volcanic hazards; calderas; peralkaline rhyolite; explosive eruptions

1. Introduction

1a. *Volcanic hazards in East Africa*

The East African Rift System (EARS) is the classic example of a continental rift system associated with active volcanism (Ebinger 2005). Magmatic systems along the densely populated EARS remain active, as demonstrated by historical eruptions (Siebert et al. 2010), active degassing (Bluth and Carn 2008; Hutchison et al. 2015; Robertson et al. 2016), recent ground deformation at multiple volcanoes (Biggs et al. 2009, 2011; Hutchison et al. 2016a; Wauthier et al. 2013), seismicity (e.g. Keir et al. 2006; Wilks et al. 2017) and ubiquitous evidence for Late Quaternary explosive eruptions in the form of tephra deposits in terrestrial and lacustrine archives (Barker et al. 2003; Blegen et al. 2015; Chalié and Gasse 2002; Fontijn et al. 2010, 2012; Hutchison et al. 2016b; Leat 1984; Le Turdu et al. 1999; Martin-Jones et al. 2017; Pyle 1999; Rapprich et al. 2016; Scott 1980). Detailed volcanic hazard assessments and/or ground-based monitoring efforts are, however, almost non-existent, raising concerns in light of population growth and the rapid expansion of geothermal infrastructure on active volcanoes (Aspinall et al. 2011; USAID 2017). A recent assessment of global volcanic risk identified Africa as a region with high population exposure combined with high vulnerability (Auker et al. 2015).

Prior studies at individual rift volcanoes in the EARS suggest late Pleistocene recurrence rate for explosive eruptions of order of 500 – 1000 years at silicic centres such as the trachytic Rungwe and Ngozi volcanoes in southern Tanzania (Fontijn et al. 2010, 2012) and the peralkaline rhyolitic complexes of Aluto (Hutchison et al. 2016b) and Corbetti (Martin-Jones et al. 2017) in Ethiopia. These long repose times and the absence of any memory of

past explosive eruptions presents challenges for the communication of volcanic hazards risk, both for local communities and the authorities (e.g. Donovan and Oppenheimer 2018).

1b. *Recent Volcanism in the Main Ethiopian Rift*

The Main Ethiopian Rift (MER) in the northernmost EARS (Fig 1), is a mature continental rift where strain is largely accommodated by magmatic intrusion and localised faulting within axial magmatic segments (Beutel et al. 2010; Casey et al. 2006; Ebinger and Casey 2001; Keranen et al. 2004). This pattern is especially well developed in the northern MER. Rifting initiated around 11 Ma in the northern MER (Wolfenden et al. 2004) and around 5-6 Ma (Bonini et al. 2005) or 8-10 Ma (WoldeGabriel et al. 1990) further south. Around 1.6-2 Ma, the distribution of activity narrowed and active faulting (Wonji Fault Belt, after Mohr 1962) and volcanism focussed within the rift floor, leading to the present-day structure (Boccaletti et al. 1998, 1999; Chernet et al. 1998; Corti 2009; Meyer et al. 1975). There is ongoing debate as to whether this shift in spatial distribution of volcano-tectonic activity results from a change in extension direction from orthogonal to oblique to the rift axis (e.g. Abebe et al. 2005; Boccaletti et al. 1998; Wolfenden et al. 2004), an increasing magmatic control over deformation (Buck 2006; Kendall et al. 2005) or continued oblique extension with pre-existing weaknesses (Corti 2008). The Wonji Fault Belt is an oblique intra-rift normal fault system which largely controls the spatial distribution of basaltic small eruptive centres (Fig 1; Abebe et al. 2007; Keir et al. 2015; Mohr 1962; Rooney et al. 2011). In this study we focus on the recent (Late Pleistocene – Holocene) explosive volcanic activity in the central MER (~7-9 °N; ~38.5-40 °E): the regularly spaced silicic (caldera) complexes on the rift axis, and the fields of small eruptive centres of mostly mafic composition (Mohr and Wood 1976; Rooney et al. 2005, 2011; Fig 1). The main centres, from North to South, are Fentale, Kone,

Boset-Bericha, Gedemsa, Bora-Baricha, Aluto, Shala and Corbetti (Fig 1; see Supplementary Table 1 for a summary, with synonyms and unique GVP code). Two zones of small eruptive centres, considered to be Late Quaternary, occur off-axis in the Bishoftu (Debre Zeyt) and Butajira areas (Fig 1; Keir et al. 2015; Rooney et al. 2011).

The late Quaternary eruption histories of central MER volcanoes are poorly known. Improved knowledge of this volcanic history is however critical to assess contemporary volcanic hazards. Several MER volcanoes are sites of active geothermal energy development (Corbetti, Aluto), with others under exploration (Fentale, Tullu Moye), adding further incentive to understand potential volcanic hazards. Within the study area, three volcanic complexes are considered to have had historical eruptions of basaltic or rhyolitic lava: Fentale (13th century AD and/or ca. 1810 AD; Section 3h), Kone (ca. 1810 AD; Section 3g) and Tullu Moye (possibly late 18th century AD and/or ca. 1900 AD; Section 3d). The presence of volcanic ash layers in lacustrine sediment cores (Chalié and Gasse 2002; Martin-Jones et al. 2017), and pumice deposits on the edifices of Aluto (Hutchison et al. 2016b) and Corbetti (Rapprich et al. 2016) volcanoes suggest the frequent occurrence of explosive eruptions in the region.

We present new field observations and geochemical data on the youngest tephra deposits from the main silicic centres of Late Quaternary volcanic activity in the central MER. We review literature data to understand the nature of recent activity at each volcano, and evaluate contemporary volcanic hazards. The scope is deliberately broad and aimed at understanding eruption frequencies and magnitudes along the MER at first order. Our observations show that the most recent stages of post-caldera activity are variable in terms of eruption frequency, magnitude and style, despite the closely similar chemical compositions of the magmas and their tectonic environments.

5

2. Field observations and geochemistry

Fieldwork along the central MER was carried out in three campaigns between 2015 and 2017. Interbedded sequences of tephra, soil and/or lacustrine deposits were logged and sampled in road cuts and gorges near Corbetti, Aluto, Bora-Baricha, Tullu Moye, Gedemsa, Boset-Bericha and Kone (Fig 1; localities in Supplementary Table 2), augmented with literature data from other MER volcanic centres.

Tephra samples were manually crushed, wet-sieved at 80 µm to remove alteration products, and dried at 50 °C. Remaining ash shards were cold-mounted in pre-drilled EpoFix resin discs, ground down with SiC paper and further polished with diamond paste. We carried out glass major element analyses on polished carbon-coated surfaces by Electron Microprobe Analysis (EMPA) using a 4-spectrometer JEOL JXA-8600 Superprobe at the Research Laboratory for Archaeology and the History of Art, University of Oxford, with an accelerating voltage of 15 kV, a defocused beam of 10 µm, and 6nA beam current. For highly vesicular samples with only small glassy surfaces, the beam size was reduced to 5 µm, and beam current lowered to 4 nA. All elements were counted on-peak for 30 s (Si, Al, Fe, Ti, Mg, Ca, K), except for Na (12 s, and analysed first to minimise alkali loss), P (60 s), Mn and Cl (50 s). Off-peak background counting times were half the peak counting times. Data quality was continuously monitored by secondary glass standards analysed at the start, regularly during (at least after every 30 unknowns) and at the end of each analytical session. Average measured values on secondary standards generally fall within 2 standard deviations of published preferred values (Jochum et al. 2006, 2011). Error bars on the measurements of unknowns were calculated using the relative standard deviation of the measured values on

6

the standard that is closest in composition to the sample. Thirty individual points were attempted per sample. Analyses were carefully screened to evaluate the potential influence of hidden crystals or voids. Only analyses with totals above 92 wt% were retained, except for samples with analytical totals systematically below 95 wt%, in which case the threshold was lowered to 90 wt%. Analytical totals are generally relatively low, typically 94-95 wt%, which can be ascribed to secondary hydration upon alteration, the presence of dissolved volatiles or other minor elements not analysed for (H_2O, F, Zr; e.g. Neave et al. 2012), and Fe_2O_3 determined as FeO (Pearce et al. 2014). Representative results for each volcanic centre are presented in Table 1; the full dataset including secondary standards is available in Supplementary Tables 3a-b. For ease of comparison, data were normalised to 100 wt% on a volatile-free basis (i.e. also excluding Cl).

3. Results: a survey of post-caldera silicic volcanism along the Main Ethiopian Rift

The new field observations, chemical data and Late Quaternary tephrostratigraphy for the silicic MER volcanoes are presented in Figures 2-13. For each volcanic complex, symbols are colour-coded across the figures showing geographic location, stratigraphy and chemistry. Summaries of the post-caldera eruptive history of each complex are presented in Table 2. Below we present our findings in the context of prior work at each volcano.

3a. Corbetti

The Corbetti complex shows evidence for a three-stage volcanic history, first recognised by Di Paola (1971): effusive shield-building, caldera collapse and, following a hiatus, post-caldera pyroclastic activity. The caldera-forming eruption(s) at Corbetti emplaced at least one unit of welded ignimbrite and associated unwelded pyroclastic deposits (Di Paola 1971;

Rapprich et al. 2013; Hutchison et al. 2016c), dated to ca. 0.18 Ma (Table 1; Hutchison et al. 2016c; WoldeGabriel et al. 1990).

At Corbetti, explosive and effusive eruptions of peralkaline rhyolite built the post-caldera edifices of Artu, Urji (or Wendo Koshe) and Chabbi (Fig 2). Artu is thought to predate both Urji and Chabbi, though no absolute chronological constraints exist (Rapprich et al. 2016). Deposits at the base of Chabbi date to ca. 20 ka (Table 1), suggesting that post-caldera activity at Corbetti has been ongoing since at least the latest Pleistocene.

Urji predominantly pumice fall and pyroclastic density current (PDC) deposits. Chabbi mainly comprises obsidian lava flows (Rapprich et al. 2016), many of which were preceded by a pyroclastic component (Mohr 1966; Di Paola 1972).. Rapprich et al. (2016) identify about a dozen events alternating between Urji and Chabbi. The most significant and widespread event is the Wendo Koshe Younger Pumice (WKYP), sourced from Urji, and dated at < 2.3 ka cal BP based on radiocarbon dating of underlying soil (Rapprich et al. 2016). Martin-Jones et al. (2017) suggest that WKYP corresponds to a 1.3-1.9 ka cal BP tephra found in sediment cores in Lakes Tilo (Fig 1, 3) and Chamo (170 km SSW of Corbetti), which is surprisingly absent from Lake Hawassa. At least four of Chabbi's obsidian flows post-date WKYP (Rapprich et al. 2016), and the Lake Tilo sediment archive suggests at least one post-WKYP explosive eruption (Fig 3; Martin-Jones et al. 2017). According to Rapprich et al. (2016) the WKYP eruption started with small-scale PDC activity and extrusion of an obsidian lava flow, followed by a sustained explosive eruption that left a distinct pumice lapilli fall deposit with an eastward dispersal pattern, and that can be found well outside the caldera. We find no evidence for obsidian lithics in the WKYP fall deposit, and suggest the obsidian lava flow may post-date the fall deposit.

Glass from Corbetti pumice has a highly uniform pantelleritic composition (Fig 3), and based on major element chemistry alone, Corbetti deposits cannot easily be distinguished. Most of our new correlations between sections are constrained by lateral tracing in the field and depositional characteristics (e.g. lithic content, or characteristic bedding). Road sections within the Corbetti Caldera reveal at least two thick pumice fall deposits separated by multiple smaller-scale fall deposits (Fig 3). Pyroclastic sequences predominantly fall deposits, with light-grey aphyric pumice and populations of dense angular obsidian clasts. Obsidian clasts are virtually absent from the WKYP, which is easily identifiable in road sections N and E of the caldera. Some deposits show systematic rhythmic bedding at cm- to dm-scale, suggesting a pulsating nature of the eruption (Fig S1b; Section 3c). In some places, small-scale PDC deposits form m-scale stacks of low-angle cross-bedded and lenticular-bedded pumice and ash units (Fig S1a). From its stratigraphic position, lateral tracing and depositional characteristics we have identified WKYP in proximal and distal sections, and have updated the dispersal map (Fig 2). The upwind and southern dispersal is poorly constrained but volume estimates using the method of Pyle (1989) suggest a minimum deposit volume of 1.3 km^3, with thicknesses of order of 0.5 m in the town of Shashemene (Fig 2). Another prominent and mostly rhythmically bedded pyroclastic deposit with obsidian clasts covers most of the eastern Urji flanks and underlies the WKYP, and is here called the Bedded Pumice. Both deposits are compositionally identical (Fig 3), but pumice textures and depositional features (massive *vs.* rhythmic bedding, presence *vs*. absence of obsidian) allow the deposits to be distinguished. Lateral tracing of thickness and maximum grain size patterns suggests the Bedded Pumice may be dispersed in a roughly circular pattern around Urji, with rhythmically-bedded packages several meters thick deposited within the caldera (Fig 2). The deposit thins rapidly to the north and south and this is

consistent with its rhythmically bedded nature resulting from pulsating behaviour gradually building a conical deposit. Other pyroclastic units exposed in sections within the caldera are of smaller scale (Fig 3).

Near the southern caldera rim, pyroclastic deposits predating the Bedded Pumice are exposed (e.g. section MER010, Fig 3-4b). The most recent unit exposed here is interpreted as Bedded Pumice because of its homogenous chemical composition as well as the occurrence of small-scale ash-rich PDC deposits covering a thin pumice fall unit, and which are also seen elsewhere. Two thick pumice lapilli breccia deposits underneath show slight compositional differences compared to the intra-caldera deposits, and can be correlated to selected ash layers from sediment cores from nearby lakes (Fig 3). A radiocarbon date on charcoal sampled from the soil underneath the oldest terrestrial deposit (MER010J; Fig 3-4b) is dated at 7.75 ± 0.04 ka cal BP (Table 3). This unit chemically resembles (slightly reduced Al_2O_3) a 6.3-8.7 ka cal BP tephra layer in Lake Tilo (TT-13), as well as the bottommost tephra in a Lake Hawassa core (AWT-7) which was dated at >7.4 ka cal BP (Martin-Jones et al. 2017). A 5.7-6.2 ka cal BP tephra in the Lake Hawassa core shows slightly elevated Al_2O_3 concentrations and can be correlated to a thick pumice fall deposit directly underlying the Bedded Pumice (Fig 3-4b).

From a composite stratigraphy of terrestrial sections we find at least 7 pyroclastic fall deposits separated by palaeosols in the last ca. 7-8 ky, 4 of which are correlated between multiple sections (e.g. MER001 and MER010; Fig 3). This is consistent with the frequency of occurrence of ash layers identified in the sediment cores from lakes Hawassa and Tilo (Martin-Jones et al. 2017; Fig 3). Sediment cores of Lake Garba Guracha, 167 km E of Corbetti in the eastern highlands (Fig 1), reportedly contain 4 tephra layers, ranging from 3

to 15 mm thick, in the last 14 kyrs (Tiercelin et al. 2008). Additional chemical data are required for verification, but the most likely source of these tephras is Corbetti. The combined terrestrial and lacustrine records thus suggest a first-order approximation of 1 explosive eruption per 700-1000 years (Martin-Jones et al. 2017; this study).

Small eruptive centres of unknown age occur immediately southeast of Corbetti, East of Lake Hawassa and North of Corbetti (red triangles on Fig 2). A rhyolitic tuff cone complex with its base ca. 40-50 m above the present-day northern shoreline of Lake Hawassa is partly onlapped by obsidian lava flows from Chabbi and surrounded by lacustrine and alluvial sediments (Rapprich et al. 2013; Fig 2). The morphology of the complex, together with the observed chaotic and heterolithic nature of its proximal deposits, mostly emplaced by PDCs (Ben Clarke, pers. comm.), suggests it may have a phreatomagmatic origin. This would be consistent with its location near the lake (e.g. Belousov and Belousova 2001; Poppe et al. 2016) although more detailed facies analyses are needed to confirm this (e.g. White and Valentine 2016). The cones east of Lake Hawassa, including one near the present-day shoreline in the city of Hawassa (Fig 2), are basaltic, and some are interpreted to have a phreatomagmatic origin (Rapprich et al. 2013). Basaltic scoria cones North of Corbetti seem to have erupted mostly along faults continuing further North to Shala Caldera (Fig 2, 5).

3b. Shala Caldera

The pre-caldera geology of the Shala caldera which contains the 250 m deep Lake Shala (Di Paola 1972) comprises deposits of rhyolitic and trachytic effusive and explosive eruptions, including extensive ignimbrites, pumice flow and pumice fall deposits exposed in the caldera

walls. Green-grey welded and unwelded ignimbrite deposits associated with the caldera-forming eruption(s) at Shala are dated at 240 ± 30 ka (bulk K-Ar; Mohr et al. 1980).

Post-caldera activity at Shala appears limited, and mostly concentrated at the Tullu Fike pumice dome complex (Fig 2). This lies outside the caldera, and is built on an apron of pumice that is 40 m thick on the northern caldera rim (Mohr et al. 1980; Fig 2). The volume of the Tullu Fike complex is ca. 3 km^3 DRE, an order of magnitude less than the cumulative post-caldera eruptive volumes of neighbouring Corbetti or Aluto (Hutchison et al. 2016c). The age of this post-caldera activity is not known, but Tullu Fike may be the source of pumice deposits interbedded with Late Quaternary lacustrine sediments in the Shala caldera walls (Mohr et al. 1980). It is not known whether any eruptive centres exist within the submerged caldera.

A few manifestations of basaltic (post-caldera?) volcanism occur in the form of isolated scoria cones in the north and a maar complex and scoria cones in the south (Mohr et al. 1980; Galo Salen unit of Trua et al. 1999; Fig 2). Some of these basaltic centres may be associated with Wonji faults cross-cutting the caldera and the area south of it, and which are in some cases also associated with hot springs (Baumann et al. 1975; Hunt et al. 2017).

3c. Aluto

The long-term magmatic evolution of the Aluto volcanic complex involves a trachytic shield-building phase, culminating in one or two caldera-forming eruptions at ca. 300-320 ka (Hutchison et al. 2016b-c). In at least the last 60 kyrs, post-caldera activity has largely filled in, and almost concealed, the caldera, with the eruption and construction of pumice cones and obsidian domes on the edifice (Fig 6; Hutchison et al. 2015, 2016b).

To the west and south-west of the complex, Late Pleistocene and Holocene pyroclastic deposits occur interbedded with lacustrine deposits related to Pleistocene and Holocene lake level high stands of the Ziway-Shala basin (Benvenuti et al. 2002, 2013; Gasse and Street 1978; Le Turdu et al. 1999). Sediment cores from nearby Lakes Abijata (Abiyata) and Langano, taken 24 km SW and 14 km S of Aluto, respectively (Fig 1), suggest the occurrence of up to 25 distinct ash horizons in the last 12 kyrs (Chalié and Gasse, 2002; Gibert et al. 1999, 2002). Aluto is the most likely source for most of these tephras, suggesting a first-order recurrence of 2-3 explosive eruptions per millennium at Aluto at least since the latest Pleistocene.

Our field observations and sampling at Aluto focused on the young pyroclastic units on the edifice (Fig S1c-d), and those interbedded with lacustrine sediments exposed in deep river gorges mainly to the west of the complex (Fig 5, 4d). These latter sections expose tens of meters thick alternations of up to 20 individual pyroclastic deposits with lacustrine deposits (diatomites) and/or palaeosols (Fig 4c). Where they are interbedded with lacustrine deposits, most of these pyroclastic deposits are dominantly clast-supported and relatively well-sorted pumice lapilli breccias at the bottom, with the appearance of a pumice fall deposit. They typically transgress upwards into a more poorly-sorted facies with more fine ash (and possibly diatomite) in the matrix (Fig 4d). Parallel bedding is common, though some units also display undulated and low-angle cross bedding in the fines-dominated parts. Occasionally matrix-supported deposits of laterally varying thickness (up to 1-2 m) and with scattered subrounded pumice clasts occur, interpreted as PDC deposits. Most deposits are interpreted to be fallout that settled through water, with their top, ash-rich parts resulting from the continued arrival of pyroclastic material deposited in the lake's catchment and remobilised as lahars (e.g. Manville et al. 2009). At ca. 8-10 km distance from the centre of

Aluto, the lowermost clast-supported parts of the deposits span thicknesses from a few cm to a few tens of dm, which are typically matched by the thickness of the upper matrix-supported parts.

Glass major element analyses of pumice lapilli and ash samples both from the main edifice and individual pyroclastic units interbedded with soils or lacustrine deposits (section A01, Fig 5) from a river gully section to the NW, shows that most pumice deposits have distinct pantelleritic compositions (Fig 6; colour-coded sample localities on Fig 5). The topmost, Qup, was previously tentatively correlated to the abundant young-looking pumice deposits occurring under the topsoil on much of the Aluto edifice (Hutchison et al. 2016b). Its distinct chemical composition however only correlates to a limited number of locations sampled across the edifice and to the west (grey dots on Fig 5, blue ones indicate samples with Qup composition; Fig 6). Rather than being the product of a single Plinian-style eruption, we infer that the previously mapped Qup unit comprises multiple pumice lapilli fall deposits sourced from different vents on the edifice. These deposits are often rhythmically bedded at a dm-scale (Fig S1d), which, together with the variety in chemical composition, is consistent with the presence of multiple pumice cones built up along the trace of the caldera ring fracture (Hutchison et al. 2015). Such pumice cones would locally have deposited thick accumulations of pumice lapilli and localised PDC deposits that overlapped, but were not widely dispersed. This is consistent with the presence of multiple moderate-scale pyroclastic deposits interbedded with the lacustrine sediments West of Aluto (Fig 4c-d, 5, S1c-d). We infer that the "true" Qup deposit, i.e. the youngest unit in section A01, and in section MER060 (Fig 5, S1c) was likely sourced from a pumice cone to the NW of the inferred caldera, and which has a prominent ca. 300 m diameter crater (Hutchison et al. 2016b). Four units underlying Qup in A01 are locally correlated in the

lacustrine and terrestrial sections to the NW of the edifice (Fig 5). Radiocarbon dating on shells incorporated in these pyroclastic and lacustrine deposits suggests the top three larger deposits, A9 (corresponding to Qup), A8 and A7 (Fig 5), to have been emplaced within the last 7,300 years (McNamara et al., unpublished data). A full integration of these sections with lake sediment cores will further improve our understanding of the frequency and magnitude of explosive eruptions at Aluto.

One sample of a 15 cm thick pumice layer with an ash matrix, taken NE of Lake Langano (pink dot on Fig 5) resembles some Corbetti glass compositions (Fig 3, 6). This pumice layer lies between two soil-and-breccia deposits, similar to those interpreted by Benvenuti et al. (2013) as early Holocene shore deposits. Gastropod shells from immediately beneath the pyroclastic unit were dated at 11.97 ± 0.09 ka cal BP (Table 3), and we suggest that this pyroclastic unit may form an early Holocene regional marker horizon from Corbetti.

Numerous scoria cones of basaltic composition have erupted along faults associated with the Wonji Fault Belt which obliquely cross-cuts the rift floor to the East of Aluto but which do not have an obvious physical connection to the complex (Fig 1, 5). With the exception of one trachyandesitic scoria cone to the NW of the complex (TAC in Fig 5) and potentially mafic components in a few (tuff) cones (all of unknown age) in the vicinity of Lake Ziway (TC in Fig 5), no clear manifestation of post-caldera mafic or intermediate volcanism is known at Aluto (Hutchison et al. 2016b; Di Paola 1972).

3d. Bora-Baricha and Tullu Moye

The low-relief complexes of Bora-Baricha and Tullu Moye, between lakes Ziway and Koka (Fig 1, 7) are poorly accessible and the least studied MER volcanoes. Welded pantelleritic

ignimbrites outcrop in the heavily faulted SE of the complex (Trua et al 1999) and have reported ages ranging from 115 ka to 1.8 Ma (fission track and K-Ar; Bigazzi et al. 1993). Remnants of caldera walls may largely be concealed by younger eruptive products. The Bora edifice is highly dissected, whereas Baricha and the Tullu Moye complex both have abundant obsidian lava flows and domes with limited soil cover, as well as hydrothermal manifestations (Fig 7; Admassu Bahiru 2007; Mengistu Darge et al. 2017).

Exploration on western and eastern sides of the complex reveals abundant silicic pyroclastic material in the form of (sometimes crudely parallel-bedded) pumice and ash fall deposits and subordinate PDC deposits. Near Baricha we find an accumulation of > 7 pumice lapilli breccia deposits alternating with poorly-developed palaeosols (section MER147; Fig 7, 8a-b). These deposits are typically characterised by a light grey dominant pumice component and a small proportion of darker grey vesicular pumice and angular obsidian chips. The pumice is a sanidine-phyric pantellerite (Fig 8c). A nearby gully exposes at least 6 more pyroclastic deposits underneath. The age of these deposits is unconstrained due to the lack of dateable material (e.g. charcoal); however the fresh appearance of the pumice and limited soil cover is consistent with a Late Quaternary age.

To the southeast of the complex, section MER150 reveals a stack of > 5 pyroclastic fall and PDC deposits, each unit multiple meters thick, and alternating with poorly-developed soils and reworked yellow ash horizons (Fig 7, 8a-b). The pumice lapilli are light grey and very phenocryst-poor to aphyric, and the deposits generally contain a few % of obsidian lithics as well as some (hydrothermally) altered lithic clasts. Several meters of subparallel cm-scale bedded poorly-sorted deposits of coarse ash, pumice and obsidian show subtle

thickness variations and minor cross-bedding in the individual beds, interpreted as dilute PDC deposits. Pumice in all units is pantelleritic, but the top unit (MER150C) is distinctive and may form a fractionation trend towards the Tullu Moye comendites (MER152; Fig 7, 8c). We suspect that the low-relief ridges and domes to the east of Bora, including the Oda crater (Fig 7), were the source of most of the deposits of MER150.

Pyroclastic deposits near Tullu Moye are typically poorly-sorted pumice lapilli and bomb breccia deposits, with angular blocks of obsidian (MER152; Fig 8b). The light grey phenocryst-poor pumice has a comenditic glass composition (Fig 8c) and often appears highly altered, with abundant secondary mineralisation. This is consistent with the persistent hydrothermal activity in the region (Mengistu Darge et al. 2017).

Poorly-vegetated obsidian lava flows near Tullu Moye (Di Paola 1972; Gouin 1979; Global Volcanism Program, http://volcano.si.edu) occur along fissures with the same strike as faults cutting through basaltic scoria cones further south as well as north towards Gedemsa (Fig 7). The youngest (least vegetated) of these obsidian flows erupted from two NNE-SSW aligned vents and formed two highly fractured > 5 m thick lava lobes; one elongate and ca. 2.7 km long by 1.6 km wide (also known as "Giano", Bizouard and Di Paola 1978), and one circular lobe ca. 1 km in diameter (darkest green lobes on Fig 7). The brecciated lava is dark grey to black and phenocryst-poor, with individual blocks showing decimetre-scale vesicular banding. Eyewitness accounts mentioned in Gouin (1979) suggest the eruption took place around 1900 AD and may have been associated with an ash fall. Bizouard and Di Paola (1978) attribute this same lava flow ("Giano") to an eruption "only two centuries ago", i.e. late 18th century AD (Siebert et al. 2010; Global Volcanism Program: http://volcano.si.edu). It is possible that both sources in fact refer to the same, poorly dated eruption. Another

young but slightly more vegetated obsidian flow occurs ca. 5 km further SSW (brightest green lobe on Fig 7) and is consistent with two recent eruptions happening in the Tullu Moye area.

3e. Gedemsa

Gedemsa is a ca. 8 km diameter and well-expressed caldera cut by the NNE-SSW trending Wonji Fault Belt along its eastern side (Fig 7). Pre-caldera products exposed on the outer flanks of the complex mostly consist of rhyolitic lava flows and domes, and pumice fall deposits (Thrall 1973; Peccerillo et al. 2003).

Light to dark grey pumice breccia deposits up to 40 m thick are described to the W of the caldera (Thrall 1973). In the north, these coarse pumice deposits alternate at a metre-scale with a few tens of cm thick packages of low-angle cross-bedded pyroclastic deposits from dilute PDCs (Fig 9a). They are overlain by a lower dark and dense, and an upper green and columnar-jointed welded ignimbrite (Thrall 1973). The green welded ignimbrite is overlain by pumice breccia deposits up to 20 m thick (Thrall 1973). The ignimbrites are typically associated to one or more caldera-forming events (Peccerillo et al. 2003), but given the volume of the underlying sequence of major unconsolidated pyroclastic deposits, including coarse pumice lapilli breccias, we suspect these latter deposits may also be related to the formation of the caldera. K-Ar dating on crystal separates of unidentified pre- and post-caldera products constrains the formation of the caldera to within 265 ± 0.02 and 319 ± 0.02 ka (Peccerillo et al. 2003). Morton et al. (1979) however present a bulk K-Ar age of 0.85 ± 0.07 Ma for a green welded tuff on the N rim of the Gedemsa caldera.

Light to dark grey pumice breccia banked up against green welded ignimbrites in the southern caldera wall (MER076A/B; Fig 7) correspond chemically to a grey pumice lapilli breccia deposit on the eastern flank of the complex (MER094A; Fig 7, 9d-e). Another poorly-sorted dark grey pumice lapilli fall deposit underlies welded ignimbrites in the NE caldera rim and on the NE flank (MER084A; Fig 7, 9a), and corresponds chemically to pyroclastic deposits exposed in a river gully to the east (MER077A/B; Fig 7, 9d-e). Here, crudely bedded dark grey fine pumice lapilli breccia interpreted as a fall deposit, is overlain by a poorly-sorted matrix-supported deposit with dispersed clasts of light grey fibrous pumice lapilli. This deposit gradually transgresses upwards into a welded facies, and is interpreted as a PDC deposit. Both deposits are separated by an ash- and lithic-rich soil suggesting a temporal hiatus. The similar chemical composition and widespread nature of the deposits however is consistent with both events being related to caldera-forming eruptions which were relatively closely spaced in time in the Late Quaternary.

Three intra-caldera coalesced domes, Kelo, Dima and Kore, are aligned WNW-ESE (Fig 7; Acocella et al. 2002) and mostly comprise poorly-sorted pumice lapilli and bomb breccias, interpreted as proximal fall deposits from the domes (Fig 9b). Kore, the easternmost centre on this alignment, has a prominent ca. 600 m diameter summit crater. Interbedded locally welded facies and obsidian lavas also occur within the deposits of these domes (Thrall 1973; Giordano et al. 2014). Several low-relief dome-shaped constructs are also identified in the northern and southern half of the caldera (Fig 7) and presumably also represent post-caldera centres of activity, though their interpretation as an eruptive volcanic feature is ambiguous.

19

Our sampling revealed at least 6 different pumice lapilli fall deposits that are geochemically distinct from the caldera-forming pyroclastic deposits (Fig 9d-e). Three of these were sampled from the proximal deposits of the intra-caldera Kore, Dima and Kelo edifices and are all pantelleritic in composition (Post-caldera cluster in Fig 9d-e). Three more geochemically unique pumice lapilli fall deposits from sections near the NE rim and E of the caldera presumably relate to additional post-caldera silicic activity, the source vents of which are however not constrained (Fig 7, 9d-e). Thicknesses of these deposits in these localities are of order of a few tens of cm.

Near the NE caldera rim, subparallel and low-angle cross-bedded poorly-sorted deposits with up to 10-15 cm clasts of scoria, basaltic lava and obsidian in an ash-rich matrix occur stratigraphically above the post-caldera pumice fall deposits (MER081A; Fig 9c-e). They are interpreted as deposits of dilute PDCs, possibly phreatomagmatic in origin. Peccerillo et al. (2003) relate them to the basaltic volcanism along the Wonji Fault Belt, with evidence for entrapment of intrusive silicic magmas from the crystallising post-caldera Gedemsa reservoir. The exact age of this activity is unknown.

Basaltic scoria cones (Peccerillo et al. 2003; Rooney et al. 2007) occur immediately NE, E and S(E) of the complex, aligned with the Wonji Faults (Fig 7). These cones lack silicic enclaves (Peccerillo et al. 2003) and are considered structurally unrelated to Gedemsa.

Immediately NW and SW of Gedemsa caldera, Thrall (1973) describes pantelleritic lava domes and local pumice deposits cut by morphologically young faults (Fig 7). It is not known whether these belong to the pre- or post-caldera stage of volcanism of the Gedemsa complex. The same faults control the location of hydrothermal springs a few km further north (Abdulkadir and Eritro 2017).

3f. Boset

Midway between Gedemsa and Boset lies the Melkassa (also known as Sodore) field of ca. 30 scoria cones around the largely eroded ca. 5 km diameter Boku caldera (Fig 10). An obsidian lava flow from this caldera was dated by Morton et al. (1979) at 0.83 ± 0.02 Ma (bulk K-Ar). The Melkassa scoria cones and associated lava flows are morphologically young and suspected to be of Late Pleistocene – Holocene age (Boccaletti et al. 1998, 1999; Siebert et al. 2010).

The Boset volcanic complex comprises two adjoining stratovolcanoes that grew along a NNE-SSE trending lineament parallel to the Wonji Fault Belt. The southern and largest of the two volcanoes is called Boset-Gudda (also "Tiliki Boset" or "Great Boset"), the northern one Boset-Bericha (also "Tinishi Boset" or "Little Boset"; Fig 10). Gudda has a 2.5 km arcuate ridge on its NW slope, which may represent the remnant of a largely infilled caldera (Di Paola 1972). In a study of the long-term evolution of the Boset volcanic complex constrained by absolute lava flow Ar-Ar chronology, Siegburg et al. (2018) constrain the caldera formation to after 119.8 ± 6.1 ka. We identified a >3.5 m thick stack of altered coarse pumice lapilli breccia and finely parallel and cross-bedded ash and small pumice lapilli deposits of dilute PDCs interbedded with palaeosols on the SE lower flank of the complex, and underneath a lava flow (outcrop MER120, Fig 10). These deposits are pantelleritic in composition, but different from the more recent pyroclastic units to the West (Fig 11). We infer the former to relate to the "ashy and pumiceous falls" described by Ronga et al. (2010) for the late-stage pre-caldera or syn-caldera activity. More dedicated studies are needed to

infer where these deposits sit in the long-term stratigraphy of the complex, and whether or not they relate to caldera-forming events.

The two central edifices of the complex mainly comprise thick trachytic and peralkaline rhyolite lava flows with associated pyroclastic deposits (Macdonald et al. 2012). These silicic lava flows have run-out distances of up to 11 km (Siegburg et al. 2018) and are often sourced from breached cones. The summit of Gudda contains a handful of NE-SW aligned small craters, up to 200-300 m diameter (blue stars on Fig 10), some with associated short obsidian lava flows (Di Paola 1972) of Holocene age (3.3 ± 2.4 ka, Ar-Ar on feldspar separates, Phase O of Siegburg et al. 2018).

Road and dry river gully sections on the Western lower flank of Boset (Fig 10) expose alternations of palaeosols and up to 6 individual pyroclastic deposits, interpreted as fall deposits, one of which is scoriaceous (Fig 11). We propose section MER108 (Fig 10-11) as the type section for the young tephrostratigraphy at Boset.

The most recent deposit is also the most voluminous and widespread, and is here called the "Boset Pumice". It comprises well-sorted pumice lapilli breccia deposits with a minor fraction of small obsidian chips, and is interpreted as a Plinian-style fall deposit. Pumice lapilli are white to light grey, very crystal-poor and have a uniform pantelleritic glass composition (Fig 11). The deposits are crudely parallel-bedded in the most proximal outcrops, where they reach thicknesses of more than 3 m and are commercially exploited. The westward distribution suggests a primary depositional thickness of order of 20 cm in the city of Adama (Fig 10). The northern and eastern (upwind) dispersal are poorly constrained but visits to outcrops along the lower Boset flanks suggest absence of the Boset Pumice deposit in these areas. A first-order approximate volume calculation using the method of

Pyle (1989) suggests a minimum deposit volume of 0.5 km^3, corresponding to a sub-Plinian eruption. From the general dispersal pattern we infer that the source vent was located on the Gudda edifice, and it may correspond to one of the craters identified as part of the youngest, Late Holocene, phase of activity at Gudda by Siegburg et al. (2018).

Recent basaltic trachyandesitic (mugearitic) lava flows were erupted from the saddle between the rhyolitic Gudda and Bericha edifices (Di Paola 1972; Brotzu et al 1974; Siegburg et al. 2018). Their whole rock composition (Brotzu et al. 1974) is very similar to that of a thin scoria fall deposit which is traceable over more than 10 km (scoria unit #2, found in MER095 and in type section MER108; Fig 10-11) and we therefore suspect the latter corresponds to an explosive phase of these mostly effusive eruptions. This is also consistent with the Holocene age (4.2 ± 3.2 ka, Ar-Ar dating on feldspar separates) constrained for one of the lava flows (Fig 10; Siegburg et al. 2018). Several scoria cones of basaltic composition occur along the NE lower flanks of the complex, and are mostly aligned NE-SW (Fig 10). Geochemical analysis on a selection of these scoria cones shows them to have similar basaltic compositions (MER109A, MER116A and MER117A; Fig 10), distinct from our scoria #2 (Fig 11). Other scoria cones occur to the SW of the complex, and are associated with the Melkassa volcanic field (Fig 10).

The basaltic trachyandesite scoria fall deposit directly overlies a lithic-poor and crystal-poor pumice fall deposit, and is intermixed in one outcrop. Both eruptions may therefore have occurred almost simultaneously. The second pumice lapilli fall (#3 in Fig 11) is markedly thinner and less widespread than the Boset Pumice, but has a similar pantelleritic composition, and is therefore likely to be sourced from Gudda (Siegburg et al. 2018). A third pantelleritic pumice fall deposit occurs underneath pumice #3. It is normally graded and

finer grained than the Boset Pumice (pumice unit #4; Fig 11). Finally, at the base of the type section MER108 (Fig 10) is a lithic-poor white pumice lapilli deposit with a distinct comenditic glass composition (Fig 11). In one section NW of the complex (MER115, Fig 10), another comenditic pumice lapilli fall deposit occurs underneath pumice #5, separated by a soil. Comenditic lava flows are only known from the Bericha edifice of the Boset complex (Siegburg et al. 2018), so we infer these lowermost comenditic pumice fall deposits to have derived from Bericha. The most recent lava flows at Bericha date to the latest Pleistocene and Holocene (Siegburg et al. 2018) and some may be associated with the comenditic pumice fall deposits.

3g. Kone

The Kone (Gariboldi in older literature) volcanic complex comprises at least three well-expressed nested calderas (Fig 12): the oldest, partially obscured Birenti Caldera which may include two nested collapse features (Cole 1969), the younger Kone Caldera and the Korke embayment (Rampey et al. 2010).

Pre-caldera activity at Birenti and Kone mostly comprises trachyte and alkali rhyolite lava flows and domes exposed in the caldera walls (Rampey et al. 2010). The caldera-forming eruptions emplaced up to several meters or tens of meters of unwelded pumice fall deposits interbedded with welded ignimbrites, typically green in colour and with varying proportions of fiamme and accidental lithics (Rampey et al. 2010). We sampled a sequence of unwelded, coarse grey pumice lapilli and bomb breccia deposits along the road between the Kone and Birenti calderas (Fig 12). We interpret these pyroclastic fall deposits as related to some of

the major events described by Rampey et al. (2010). Major element glass chemistry suggests three distinct comenditic to pantelleritic compositions (Fig 13). We infer the comenditic pumice, sampled from three localities along the N rim of the Korke embayment, to be associated with the Kone caldera forming event(s) (unit Qpk, after Rampey et al. 2010). The pantelleritic pumice may represent other units within the Kone pyroclastic sequence, or other phases from the Kone Caldera Complex. MER141A (yellow symbols in Fig 12-13) may correspond to a non-welded pyroclastic facies of the Birenti caldera-forming events (units Qub or Qim, Rampey et al. 2010). MER130A (blue symbols in Fig 12-13), a poorly-sorted, >2.5 m thick grey coarse pumice lapilli and bomb breccia deposit, may correspond to the pyroclastic deposits associated with a post-caldera rhyolitic dome on the southern Kone caldera wall (units Qrd and Qpd, Rampey et al. 2010).

The age and detailed stratigraphy of these events remains poorly constrained, and it is unclear which eruption formed the Korke embayment (Rampey et al. 2010). Williams et al. (2004) show a schematic section near the SE margin of the Kone caldera, where a welded ignimbrite and overlying ash (flow?) and pumice fall deposits lie beneath a Middle Stone Age palaeosol (> 200 ka; Basell 2008; Williams et al. 2004). Without additional spatial and geochemical data it is not possible to assign a correlation with any of the pyroclastic deposits described by Rampey et al. (2010).

In a study of Middle Stone Age obsidian tool provenance, potential obsidian source rocks sampled near the NE rim of the Kone caldera were Ar-Ar–dated at 391 ± 2 and 395 ± 6 ka (Vogel et al. 2006). Glass geochemical data on these same black to deep green obsidian source rocks (Negash et al. 2007) are closely similar to MER141A (yellow symbols in Fig 12-13), and may put a temporal constraint on the formation of these deposits.

Rampey et al. (2010) describe the few post-caldera silicic lava flows and domes which erupted along the southern and northern Kone caldera rims, and along NE-SW oriented faults north of the complex. Sparse pyroclastic deposits are also associated with the caldera ring fault (and may correspond to MER130A, blue symbols in Fig 12-13, see above), but the age of these eruptions is unconstrained, and it is unclear whether they are representative of the contemporary volcanism at the Kone Caldera complex. In our reconnaissance visit we did not find any evidence for fresh-looking loose pyroclastic deposits of silicic composition.

Recent basaltic lava flows erupted from NE-SW aligned scoria cones on the hinge between the Kone and Korke calderas, filling both caldera floors (Acocella et al. 2002). The most recent of these events may have occurred historically, with many secondary sources suggesting an eruption date of ca. 1810-1830 AD (e.g. Buxton 1949; Cole 1969), originally derived from the accounts of Harris (1844). In April 1842, Harris visited the "crater of Saboo" (Sabober, S of Fentale; Fig 12), which was "said to have been in full activity in the time of Sahela Selassie's grandsire" (Harris 1844, p. 255). Selassie's grandfather, Asfaw Wossen, was ruler of Shoa from 1774-1808 (Keynes 2007). Harris also visited Kone, which he describes as "the crater of Winzegoor", and where he noted that the fresh lavas were still "jet black", and that two "bare truncated cones" erupted "some thirty years previously" remained dark and cindery. One reading of Harris' accounts is that there was an episode of mafic rift-floor volcanism extending between Kone and Fentale, similar to the Dabbahu – Manda Hararo rifting episode from 2005-2010 (e.g. Ferguson et al. 2010), and that this had a peak in the later parts of Asfaw Wossen's reign, perhaps ca. 1800-1808. Other morphologically fresh and poorly vegetated, blocky basaltic lava flows occur to the N and NE of the caldera complex, most notably to the N of a large scoria cone, Beru (Fig 13). Our glass geochemical analyses confirm the basaltic composition for these recent scoria cones (Fig 12-13).

3h. Fentale

Fentale is the northernmost MER volcano, at the junction with the Afar depression, and hosts a ca. 2.5 by 4 km diameter summit caldera elongated NNW-SSE (Fig 12). The green welded ash-flow tuff of Fentale that was emplaced by the caldera-forming eruption is dated at 168 ± 38 ka by fission track dating on the glass (Williams et al. 2004). Based on the chemical composition of different flow units identified within the ash-flow tuff, Gibson (1974) suggested the related eruption emptied a chemically zoned magma chamber with a trachytic base and rhyolitic top. On the southern flank, the welded tuff deposit has distinctive blisters, sometimes up to 100 m in diameter, presumably formed by degassing of large coalesced gas pockets within the newly emplaced deposit (Gibson 1970).

Post-caldera eruptions of obsidian and rhyolite lava flows were sourced from NNW-SSE aligned vents and fissures within the caldera (Acocella et al. 2002), as well as on the NE, E, SE and W flanks of the volcano (Williams et al. 2004; Gibson 1974). The morphologically youngest and most poorly vegetated obsidian flow was erupted from a vent within the caldera. Some post-caldera eruptions emplacing obsidian lava flows possibly also had an explosive phase, as evident from fresh superficial pumice lapilli scattered around the lower slopes of Fentale. There is however no evidence for significant silicic explosive volcanism emplacing widespread pumice fall deposits in the post-caldera stage at Fentale.

Basaltic activity near Fentale occurs immediately South of the edifice. A basaltic tuff cone, Tinish Sabober (Williams et al. 2004; Fig 12) is covered on its flanks with a veneer of welded tuff from the caldera-forming eruption, hence pre-dates it (Gibson 1967, 1974). Much more recent basaltic activity has occurred in the same region with the emission of

lava flows from fissures and small cones aligned NE-SW with the centre of the tuff cone (Williams et al. 2004). Local oral tradition reported by Harris (1844, p255) suggests activity during the reign of Asfaw Wossen, who died in 1808 (Keynes 2007; Section 3g). The fresh and almost non-vegetated nature of the Fentale basaltic lava flows, similar to those at the Kone caldera complex, does suggest they may have erupted historically.

A poorly documented "13th century" eruption of Fentale is reported in Newhall and Dzurisin (1988), after Azais and Chambord (1931), who record an account by a priest mentioning the destruction of a church and town near present-day Lake Metehara (also known as Lake Beseka, Fig 12). It is unclear whether this event could actually relate to the 19th century lava flows, given their geographic location close to the lake, or whether it represents an eruption from a vent elsewhere on the edifice.

3i. Off-axis volcanism

Our evaluation of recent volcanism in the MER is focussed on the on-axis volcanic centres within the MER, which are generally assumed to be the locus of most of the present-day volcanic and tectonic activity (e.g. Corti 2009; Keir et al. 2015). Off-axis volcanism occurs as small eruptive centres of mainly basaltic composition in the Bishoftu (Debre Zeyt) and Butajira volcanic fields on the Western rift shoulder (Fig 1; Rooney et al. 2005, 2011). In the Bishoftu area several phreatomagmatic vents (maars) exist and these comprise pumiceous tuff deposits (Emilia et al. 1977). This off-axis volcanism is generally assumed to be Late Quaternary in age because of its morphologically young appearance, though absolute chronologies or modern evaluations of their potential future hazards are lacking. To the

southern end of the Bishoftu area, the large silicic volcano of Ziquala (Zuquala) dominates the landscape, and has a prominent summit crater hosting a lake. Trachytic lavas from the base, flank and rim of the volcano were dated (K-Ar on feldspar separates) between 0.85 ± 0.05 and 1.28 ± 0.15 Ma (Morton et al. 1979) but its youngest eruptive products have not been studied.

4. Discussion

4a. Diversity in style and rate of silicic volcanism along the MER

The timing of caldera-forming eruptions and initiation of post-caldera activity along the MER is still relatively poorly constrained, with the exception of recently re-evaluated ages at Aluto and Corbetti using high-precision sanidine Ar-Ar dating as opposed to bulk K-Ar dating (Hutchison et al. 2016c). In this study we focus mainly on the youngest post-caldera activity at each MER centre as constrained by field observations. Post-caldera Late Quaternary activity along the MER is dominated by effusive and/or explosive eruptions of peralkaline rhyolitic magmas, generating obsidian flows and domes and pumice cones within the old calderas, at all centres except Kone (Table 2).

Corbetti and Aluto have both been highly active in the Late Quaternary, as evidenced by the presence of numerous volcanic ash layers in lacustrine sediment cores spanning the last 12,000 years (Chalié and Gasse 2002; Martin-Jones et al. 2017), and multiple pumice fall deposits on their edifices. Deposits of these explosive eruptions are moderately widespread, with some suggesting up to sub-Plinian scale magnitudes (typically VEI 3-4, which would correspond to deposit volumes of order of 0.1 km^3; Newhall and Self 1982; Pyle 2015, 2016). The best documented and youngest deposit in our record from Aluto presented here, Qup,

is almost 3 meters thick near its presumed source vent, but rapidly thins away to a few tens of cm or even less within 5 km distance both to the W and E (Fig 5). Deposits of similar scale are also found at Tullu Moye and Boset-Bericha. At Gedemsa and possibly also at Tullu Fike near the Shala Caldera, we find more localised coarse pumice bomb breccia deposits representing post-caldera stage explosive activity (Table 2).

The metre- to decimetre-thick proximal pyroclastic fall deposits found at Corbetti, Bora-Baricha and Boset-Bericha are consistent with larger, VEI 4-5 eruptions generating deposit volumes of ca. 1 km^3 (Newhall and Self 1982; Pyle 2015, 2016). At Corbetti there is evidence for two such Holocene events, in addition to multiple smaller-scale explosive eruptions (Fig 3), some of them possibly associated with the effusion of obsidian lava flows. Proximal-medial multiple-metre thicknesses of pumice fall deposits from Bora and/or Baricha are also consistent with eruptions up to VEI 5. Limited accessibility prevents us from obtaining more detailed magnitude estimates for the scale of these important eruptions. The most prominent recent explosive eruption of the Boset-Bericha complex was that of the sub-Plinian "Boset Pumice".

Conservative estimates of VEI 3-4 eruptions and corresponding minimum deposit volumes of 0.01 km^3 and 0.1 km^3 (Pyle 2015, 2016) allow us to semi-quantitatively constrain first-order eruptive rates in the Holocene for some MER volcanoes. Based on the rapid thinning trends of Qup (Fig 5; see above) we assign a magnitude of 3 to all of the 25 Aluto deposits in the last 12,000 years (Table 2) and a magnitude of 4 to 4 of the 7, and magnitude 3 to the 3 remaining, Corbetti eruptions constrained on land (based on relative thicknesses in the proximal sections; Fig 3). This results in a minimum estimate of volumetric eruptive rates of 0.01 – 0.1 km^3 / ky at these two volcanoes (assuming 800 kg/m^3 of deposit density,

and 2380 kg/m^3 peralkaline rhyolite density, in the absence of other constraints from e.g. water content; Neave et al. 2012), substantially less than the 0.5 – 0.75 km^3 / ky constrained for the mid-Pleistocene "silicic flare-up" in the CMER (primarily Aluto and Corbetti), the period during which most of the calderas were formed (Hutchison et al. 2016c). These modern eruptive rates are also lower but broadly comparable with those estimated for the highly explosive trachytic Rungwe and Ngozi volcanoes in southern Tanzania (ca. 0.25 km^3 / ky; Fontijn et al. 2010, 2012). Note that the above estimates (except for the "flare-up" ones of Hutchison et al. 2016c) do not take into account the effusive eruptive products and are based on minimum eruptive volumes, therefore represent minimum rates.

At Aluto and Corbetti most of the obsidian lava flows and *coulées* are presumably associated with an explosive eruption either preceding or following the effusive phase (Hutchison et al. 2016b; Di Paola 1972). This is consistent with the ubiquitous presence of pumice deposits on both edifices, and is observed on other peralkaline volcanoes producing pumice cones and obsidian lavas (Dellino and La Volpe 1995; Mahood and Hildreth 1986). Further north along the MER, at Tullu Moye, but particularly Boset-Bericha and Fentale there is a generally increasing proportion of silicic effusive (obsidian lava flows) over explosive volcanism. At Tullu Moye several of the most recent silicic eruptions have been effusive and emplaced thick obsidian lava flows. We did not encounter evidence of an associated explosive eruption, though the historical accounts of the youngest eruption do suggest the occurrence of ash fall (Gouin 1979). The strongly fault-controlled Boset-Bericha complex has experienced both effusive and a limited number of explosive eruptions in its most recent phases, with most of the edifices built up by silicic lava flows (Fig 10; Siegburg et al. 2018). At Fentale, silicic post-caldera volcanism seems dominated by obsidian lava flows, possibly with a small component of associated explosive activity.

4b. Volcano-tectonic interactions and mafic volcanism along the MER

Active faults of the Wonji Fault Belt cross-cutting Fentale, Kone and Gedemsa facilitate the eruption of basaltic magmas, forming scoria cones and lava flows. At Kone, post-caldera activity is entirely dominated by such small-scale basaltic lava flows and scoria-cone-building eruptions and no silicic products are identified in the post-caldera stage. Also at Gedemsa, the youthful nature of the faults cross-cutting the eastern sector of the caldera, and their aligned scoria cones (Fig 7), are indicative of a predominance of basaltic volcanism over silicic volcanism in the present stage. It has been suggested that the post-caldera basaltic products at these three volcanic complexes should not be considered as part of their respective predominantly silicic complexes, but represent a renewed phase of basaltic activity purely related to the Wonji Fault Belt (Giordano et al. 2014; Gibson 1974).

At Tullu Moye and Boset-Bericha, the Wonji Fault Belt however controls the eruption of both mafic and silicic magmas, which have clearly erupted contemporaneously in the recent past (Fig 7, 10-11; Siegburg et al. 2018). The southernmost clear surface expression of the Wonji Fault Belt is the field of basaltic scoria cones east of Lake Ziway (Fig 1). Whereas this basaltic volcanism is generally assumed to be cogenetic with the silicic products erupted from the post-caldera edifice of Aluto (Hutchison et al. 2016b), the detailed spatial and temporal relationships are not well constrained.

At Aluto and Corbetti all the basaltic (and presumably post-caldera) surface manifestations of volcanism occur well outside the known extent of the calderas and this may reflect the presence of a higher proportion of silicic melt in the crust relative to some of the other systems where basalt erupts along fractures cross-cutting the calderas (Kone,

Gedemsa). The larger amounts of silicic crustal melt would in this case prevent the denser basaltic melt to rise up through the caldera and instead deflect it to a "shadow zone" outside the caldera (e.g. Hutchison et al. 2016a; Mahood 1984; Mahood and Hildreth 1986; Jeffery et al. 2016).

4c. Implications for volcanic hazards

Our tephrostratigraphic records for Aluto and Corbetti provide evidence for explosive eruptions at these volcanoes in the Holocene of up to 1-3 explosive events per millennium. Most of these eruptions have been of moderate scale but especially at Corbetti, some appear to be VEI 4-5. The largest Holocene explosive eruptions in the MER deposited several tens of centimetres of pumice and ash in areas which today are densely populated rural areas or urbanised population centres. The Boset Pumice eruption generated a pumice fall deposit of >0.5 km^3, with a deposit thickness of ca. 20 cm in the city of Adama. The most recent large eruption at Corbetti (WKYP) shows a Plinian-style elliptical dispersal pattern, with a dispersal axis to the E and deposition of ca. 50 cm of pumice fall in the town of Shashemene and possibly more than 10 cm in the city of Hawassa (Fig 2). Such deposit thicknesses are sufficient to cause widespread damage and disruption to infrastructure and agriculture (e.g. Ayris and Delmelle 2012; Wilson et al. 2012). The dispersal axes as constrained from these deposits are not all consistent with the present-day dominant wind directions at this latitude (very minor to the SW or NE) but this may be due to the close proximity to the Intertropical Convergence Zone and its possible shifts throughout the Late Quaternary (e.g. Gasse 2000; Lézine et al. 2017).

The Bedded Pumice deposit of a large explosive eruption of Corbetti preceding WKYP has entirely overlapping major element composition (Fig 3), and shows rapid thinning away from the vent (i.e. more cone-like deposition, in contrast to sheet-like for WKYP; Fig 2). This is consistent with the rhythmically-bedded nature of its proximal deposits, which have built up a pumice cone (Fig S1b). Such crude parallel bedding, typically represented as gradual alternations of fine and coarser pumice lapilli at a dm-scale, reflects temporal variations in eruptive intensity and is commonly found in the pyroclastic fall deposits of most MER volcanoes and other peralkaline rhyolite volcanoes such as Pantelleria (Orsi et al. 1991) or Monte Pilato (Lipari; Davì et al. 2011) in Italy. These variations may reflect a typical pulsating style of activity controlled by the degassing dynamics in these moderately low-viscosity, crystal-poor magmas (Di Carlo et al. 2010; Di Genova et al. 2013; Neave et al. 2012); however the eruption dynamics, including initiation, evolution and duration of events, and resulting tephra dispersal patterns of pumice cone forming eruptions remain poorly understood.

4d. Chronology and preservation

In the latest Pleistocene and Holocene timeframe, the scarcity of useful material for radiocarbon dating (e.g. charcoal embedded in pyroclastic deposits) from terrestrial sections in the MER provides a great challenge to constrain absolute chronologies and eruptive rates of silicic *vs.* mafic volcanism. In the absence of absolute chronologies, subtle variations in glass major element chemical composition between otherwise similar deposits allow us to fingerprint units and constrain relative stratigraphies and minimum amounts of eruptive events in the recent geological past. At some volcanoes however, additional chemical data

such as glass trace element or mineral major element composition (e.g. Albert et al. 2012; Rawson et al. 2015) might allow us to refine correlations in addition to stratigraphic constraints.

The most detailed records of Late Quaternary eruptions are from settings where pyroclastic deposits are interbedded with lacustrine deposits containing macrofossil remains (Corbetti, Aluto). At Aluto, the Late Quaternary pyroclastic – lacustrine sequences exposed on land as a result of extensive lake level fluctuations (Benvenuti et al. 2002, 2013; Le Turdu et al. 1999) provide scope to integrate these sequences with lake sediment cores (Chalié and Gasse 2002) into a robust chronological framework that allows the study of temporal variations in and interactions between volcanism, tectonic activity and the palaeoenvironment.

Deposition of pyroclastic deposits in lakes may favour their preservation in the geological record, as the terrestrial environment is more prone to weathering and erosion; and it is well known that lacustrine sequences tend to preserve more complete records of volcanism than terrestrial sequences alone (e.g. Bertrand et al. 2014; Fontijn et al. 2016; Green et al. 2016). The lack of exposed lacustrine sequences North of Aluto does therefore potentially bias the preserved record to the largest of events. Note, however, that apart from near Aluto, most of our studied sections at all the other volcanoes are in fact terrestrial. It is possible that the relatively small-scale (e.g. VEI 3 and below) events are missing from these sequences, but we would expect abundant evidence for VEI 4 and above events to be preserved in soil sequences had they occurred in the recent geological past (e.g. Brown et al. 2014; Fontijn et al. 2010; Pyle 2016).

The new geochemical data and observations of proximal pyroclastic deposits from all the major silicic MER volcanic complexes presented in this paper will allow improved tephrochronological correlations between Late Quaternary sedimentary archives across central Ethiopia (e.g. Martin-Jones et al. 2017; Tiercelin et al. 2008). Such regional-scale correlations of proximal with more distal records will in return allow the fine-tuning of our eruptive chronologies and frequencies, as well as constrain eruption magnitudes and dispersal patterns important for future hazard assessment. Studies limited to tephras in lacustrine settings (e.g. Martin-Jones et al. 2017) may provide constraints on frequencies of events, but cannot highlight the complexity and diversity of eruptive styles and eruption dynamics. At best such studies are complementary to field-based volcanology to understand volcanic hazards. It is critical that this complexity is well-documented, including from detailed field observations of proximal deposits, before undertaking hazard assessments that ultimately feed into risk management policies.

5. Conclusions

Geological evidence and current geophysical unrest at many (Biggs et al. 2011; Hutchison et al. 2016a) on-axis silicic MER volcanoes suggests that they remain active and are likely to erupt again in the future. Here we present new fieldwork and geochemical data of late Quaternary silicic tephra deposits in the MER. Our work suggests that potential volcanic hazards and risks at the central MER silicic caldera systems vary widely between each complex, despite similarities in their structure, chemical composition and long-term evolution. Corbetti and Aluto have both been highly active in the Late Quaternary. Their eruption frequencies of 1-3 events per millennium place them amongst the most frequently

active volcanoes for moderate-scale explosive eruptions in East Africa. Some recent MER eruptions were of sub-Plinian scale, depositing tens of centimetres of pumice and ash at present-day densely populated rural areas as well as urbanised population centres. In addition to evidence of explosive activity, most silicic MER complexes have also experienced recent silicic effusive activity in the form of thick obsidian lava flows. The striking variety of eruptive style and rates at the seemingly similar volcanoes along the MER requires a detailed evaluation of volcanic hazard and risk at a regional scale in this (and other) part(s) of the East African Rift System to incorporate reconnaissance studies on each individual centre, and questions the use of analogies to inform hazard and risk mitigation policies.

Acknowledgements

such as settlements and lakes, and topography were retrieved from http://naturalearthdata.com. Editorial handling by Kelly Russell and reviews by Karoly Nemeth and an anonymous reviewer were greatly appreciated.

References

Abdulkadir, Y.A., Eritro, T.H., 2017. 2D resistivity imaging and magnetic survey for characterization of thermal springs: A case study of Gergedi thermal springs in the northwest of Wonji, Main Ethiopian Rift, Ethiopia. Journal of African Earth Sciences, 133: 95-103.

Admassu Bahiru, E., 2007. Structural study and its effect on thermal activities of Tulu Moye – Gedemsa Area. Master of Science Thesis, Addis Ababa University, Department of Earth Sciences, 88pp.

Abebe, B., Acocella, V., Korme, T. & Ayalew, D., 2007. Quaternary faulting and volcanism in the Main Ethiopian Rift. Journal of African Earth Sciences, 48: 115 - 124.

Abebe, T., Manetti, P., Bonini, M., Corti, G., Innocenti, F., Mazzarini, F. and Pecksay, Z., 2005. Geological map (scale 1:200,000) of the northern Main Ethiopian Rift and its implications for the volcano-tectonic evolution of the rift. Geological Society of America Map and Chart Series, MCH094.

Acocella, V., Korme, T., Salvini, F. and Funiciello, R., 2002. Elliptic calderas in the Ethiopian Rift: control of pre-existing structures. Journal of Volcanology and Geothermal Research, 119(1–4): 189-203.

Albert, P.G., Tomlinson, E.L., Smith, V.C., Di Roberto, A., Todman, A., Rosi, M., Marani, M., Muller, W. and Menzies, M.A., 2012. Marine-continental tephra correlations: Volcanic glass geochemistry from the Marsili Basin and the Aeolian Islands, Southern Tyrrhenian Sea, Italy. Journal of Volcanology and Geothermal Research, 229–230: 74-94.

Aspinall, W., Auker, M., Hincks, T., Mahony, S., Nadim, F., Pooley, J., Sparks, S. and Syre, E.,

2011. Volcano Hazard and Exposure in GFDRR Priority Countries and Risk Mitigation Measures. NGI Report 20100806, World Bank - Global Facility for Disaster Reduction and Recovery, 309pp

Auker, M.R., Sparks, R.S.J., Jenkins, S.F., Aspinall, W., Brown, S.K., Deligne, N.I., Jolly, G., Loughlin, S.C., Marzocchi, W., Newhall, C.G., Palma, J.L., 2015. Development of a new global Volcanic Hazard Index (VHI). In: Loughlin, S.C., Sparks, S., Brown, S.K., Jenkins, S.F., Vye-Brown, C. (eds) *Global Volcanic Hazards and Risk*. Cambridge University Press, pp. 349–358

Ayris, P.M. and Delmelle, P., 2012. The immediate environmental effects of tephra emission. Bulletin of Volcanology, 74(9): 1905-1936.

Azais, R.P., Chambord, P., 1931. Cinq années de recherches archéologiques en Ethiopie. Paris, 142pp.

Barker, P., Williamson, D., Gasse, F. & Gibert, E., 2003. Climatic and volcanic forcing revealed in a 50,000-year diatom record from Lake Massoko, Tanzania. Quaternary Research, 60: 368 - 376.

Basell, L.S., 2008. Middle Stone Age (MSA) site distributions in east Africa and their relationship to Quaternary environmental change, refugia and the evolution of *Homo sapiens*. Quaternary Science Reviews, 27: 2484-2498.

Baumann, A., Förstner, U. and Rohde, R., 1975. Lake Shala: Water chemistry, mineralogy and geochemistry of sediments in an Ethiopian Rift lake. Geologische Rundschau, 64(1): 593-609.

Belousov, A. and Belousova, M., 2001. Eruptive process, effects and deposits of the 1996 and the ancient basaltic phreatomagmatic eruptions in Karymskoye Lake, Kamchatka, Russia. Special Publication of the International Association of Sedimentologists, 30: 35-60.

Benvenuti, M., Bonini, M., Tassi, F., Corti, G., Sani, F., Agostini, A., Manetti, P. and Vaselli, O., 2013. Holocene lacustrine fluctuations and deep CO2 degassing in the northeastern Lake Langano Basin (Main Ethiopian Rift). Journal of African Earth Sciences, 77: 1-10.

Benvenuti, M., Carnicelli, S., Belluomini, G., Dainelli, N., Di Grazia, S., Ferrari, G.A., Iasio, C.,

Sagri, M., Ventra, D., Atnafu, B. and Kebede, S., 2002. The Ziway–Shala lake basin (main Ethiopian rift, Ethiopia): a revision of basin evolution with special reference to the Late Quaternary. Journal of African Earth Sciences, 35(2): 247-269.

Bertrand, S., Daga, R., Bedert, R. and Fontijn, K., 2014. Deposition of the 2011–2012 Cordón Caulle tephra (Chile, 40°S) in lake sediments: Implications for tephrochronology and volcanology. Journal of Geophysical Research: Earth Surface, 119: 2555-2573.

Beutel, E., van Wijk, J., Ebinger, C., Keir, D., Agostini, A., 2010. Formation and stability of magmatic segments in the Main Ethiopian and Afar rifts. Earth and Planetary Science Letters, 293: 225 - 235.Bigazzi, B., Bonadonna, F.P., Di Paola, G.M. and Giuliani, A., 1993. K-Ar and fission track ages of the last volcano tectonic phase in the Ethiopian Rift Valley (Tullu Moye' Area), Geology and mineral resources of Somalia and surrounding region, pp. 311-322.

Biggs, J., Anthony, E.Y. and Ebinger, C.J., 2009. Multiple inflation and deflation events at Kenyan volcanoes, East African Rift. Geology, 37(11): 979-982.

Biggs, J., Bastow, I.D., Keir, D. and Lewi, E., 2011. Pulses of deformation reveal frequently recurring shallow magmatic activity beneath the Main Ethiopian Rift. Geochemistry, Geophysics, Geosystems, 12(9): Q0AB10.

Bizouard, H., Di Paola, G.M., 1978. Mineralogy of the Tullu Moje active volcanic area (Arussi: Ethiopian Rift Valley). In: Neumann, E.R., Ramberg, I.B. (eds) *Petrology and Geochemistry of Continental Rifts*, Reidel Publishing Company, Dordrecht, Holland, pp. 87–100.

Blegen, N., Tryon, C.A., Faith, J.T., Peppe, D.J., Beverly, E.J., Li, B. and Jacobs, Z., 2015. Distal tephras of the eastern Lake Victoria basin, equatorial East Africa: correlations, chronology and a context for early modern humans. Quaternary Science Reviews, 122: 89-111.

Bluth, G.J.S., Carn, S.A., 2008. Exceptional sulphur degassing from Nyamuragira volcano, 1979-2005. International Journal of Remote Sensing 29:6667–6685. http://dx.doi.org/10.1080/0143116802168434.

Boccaletti, M., Bonini, M., Mazzuoli, R., Abebe, B., Piccardi, L. and Tortorici, L., 1998.

Quaternary oblique extensional tectonics in the Ethiopian Rift (Horn of Africa). Tectonophysics, 287(1): 97-116.

Boccaletti, M., Mazzuoli, R., Bonini, M., Trua, T. and Abebe, B., 1999. Plio-Quaternary volcanotectonic activity in the northern sector of the Main Ethiopian Rift: relationships with oblique rifting. Journal of African Earth Sciences, 29(4): 679-698.

Bonini, M., Corti, G., Innocenti, F., Manetti, P., Mazzarini, F., Abebe, T. and Pecskay, Z., 2005. Evolution of the Main Ethiopian Rift in the frame of Afar and Kenya rifts propagation. Tectonics, 24(1).

Bronk Ramsey, C., 2009. Bayesian analysis of radiocarbon dates. Radiocarbon, 51(1): 337 - 360.

Brotzu, P., Morbidelli, L., Piccirillo, E.M. and Traversa, G., 1974. Petrological features of boseti mountains, a complex volcanic system in the axial portion of the main Ethiopian rift. Bull Volcanol, 38(1): 206-234.

Brown, S., Crosweller, H., Sparks, R., Cottrell, E., Deligne, N., Guerrero, N., Hobbs, L., Kiyosugi, K., Loughlin, S., Siebert, L. and Takarada, S., 2014. Characterisation of the Quaternary eruption record: analysis of the Large Magnitude Explosive Volcanic Eruptions (LaMEVE) database. Journal of Applied Volcanology, 3(5): 22.

Buck, W.R., 2006. The role of magma in the development of the Afro-Arabian Rift System. Geological Society, London, Special Publications, 259(1): 43-54.

Buxton, D.R., 1949. Travels in Ethiopia. Drummond, London, 200pp

Casey, M. Ebinger, C., Keir, D., Glouaguen, R., Mohamed, F., 2006. Strain accommodation in transitional rifts: extension by magma intrusion and faulting in Ethiopian rift magmatic segments. In: Yirgu, G., Ebinger, C.J., Maguire, P.K.H. (eds) *The Afar Volcanic Province within the East African Rift System*. Geological Society of London Special Publications 259:143–164.

Chalié, F. and Gasse, F., 2002. Late Glacial–Holocene diatom record of water chemistry and lake level change from the tropical East African Rift Lake Abiyata (Ethiopia). Palaeogeography, Palaeoclimatology, Palaeoecology, 187(3–4): 259-283.

Chernet, T., Hart, W.K., Aronson, J.L. and Walter, R.C., 1998. New age constraints on the

timing of volcanism and tectonism in the northern Main Ethiopian Rift–southern Afar transition zone (Ethiopia). Journal of Volcanology and Geothermal Research, 80(3–4): 267-280.

Cole, J.W., 1969. Gariboldi volcanic complex, Ethiopia. Bull Volcanol, 33(2): 566-578.

Corti, G., 2008. Control of rift obliquity on the evolution and segmentation of the main Ethiopian rift. Nature Geosci, 1(4): 258-262.

Corti, G., 2009. Continental rift evolution: From rift initiation to incipient break-up in the Main Ethiopian Rift, East Africa. Earth Science Reviews, 96: 1-53.

Davì, M., De Rosa, R., Donato, P. and Sulpizio, R., 2011. The Lami pyroclastic succession (Lipari, Aeolian Islands): A clue for unravelling the eruptive dynamics of the Monte Pilato rhyolitic pumice cone. Journal of Volcanology and Geothermal Research, 201(1–4): 285-300.

Dellino, P. and Volpe, L.L., 1995. Fragmentation versus transportation mechanisms in the pyroclastic sequence of Monte Pilato-Rocche Rosse (Lipari, Italy). Journal of Volcanology and Geothermal Research, 64(3–4): 211-231.

Di Carlo, I., Rotolo, S.G., Scaillet, B., Buccheri, V. and Pichavant, M., 2010. Phase Equilibrium Constraints on Pre-eruptive Conditions of Recent Felsic Explosive Volcanism at Pantelleria Island, Italy. Journal of Petrology, 51(11): 2245-2276.

Di Genova, D., Romano, C., Hess, K.U., Vona, A., Poe, B.T., Giordano, D., Dingwell, D.B. and Behrens, H., 2013. The rheology of peralkaline rhyolites from Pantelleria Island. Journal of Volcanology and Geothermal Research, 249: 201-216.

Di Paola, G.M., 1971. Geology of the Corbetti Caldera area (Main Ethiopian Rift Valley). Bull Volcanol, 35(2): 497-506.

Di Paola, G.M., 1972. The Ethiopian Rift Valley (between 7° 00' and 8° 40' lat. north). Bull Volcanol, 36(4): 517-560.

Donovan, A. and Oppenheimer, C., 2018. Imagining the Unimaginable: Communicating Extreme Volcanic Risk. In: Bird, D., Jolly, G., Haynes, K., McGuire, B., Fearnley, C. (eds) Volcanic Crisis Communication: Observing the Volcano World. Springer IAVCEI series Advances in Volcanology, Berlin, Heidelberg, doi 10.1007/11157_2015_16.

Ebinger, C., 2005. Continental break-up: The East African perspective. Astronomy & Geophysics, 46: 2.16 - 12.21.

Ebinger, C.J. and Casey, M., 2001. Continental breakup in magmatic provinces: An Ethiopian example. Geology, 29(6): 527-530.

Emilia, D.A., Last, B.J., Wood, C.A. and Dakin, F.M., 1977. Geophysics and geology of an explosion crater in the Ethiopian rift valley. Bull Volcanol, 40(3): 133-140.Ferguson, D.J., Barnie, T.D., Pyle, D.M., Oppenheimer, C., Yirgu, G., Lewi, E., Kidane, T., Carn, S. and Hamling, I., 2010. Recent rift-related volcanism in Afar, Ethiopia. Earth and Planetary Science Letters 292: 409-418

Fontijn, K., Ernst, G.G.J., Elburg, M.A., Williamson, D., Abdallah, E., Kwelwa, S., Mbede, E., Jacobs, P., 2010. Holocene explosive eruptions in the Rungwe Volcanic Province, Tanzania. Journal of Volcanology and Geothermal Research, 196: 91 - 110.

Fontijn, K., Rawson, H., Van Daele, M., Moernaut, J., Abarzúa, A.M., Heirman, K., Bertrand, S., Pyle, D.M., Mather, T.A., De Batist, M., Naranjo, J.-A. and Moreno, H., 2016. Synchronisation of sedimentary records using tephra: A postglacial tephrochronological model for the Chilean Lake District. Quaternary Science Reviews, 137: 234-254.

Fontijn, K., Williamson, D., Mbede, E. and Ernst, G.G.J., 2012. The Rungwe Volcanic Province, Tanzania – A volcanological review. Journal of African Earth Sciences, 63(0): 12-31.

Gasse, F., 2000. Hydrological changes in the African tropics since the Last Glacial Maximum. Quaternary Science Reviews, 19: 189-211.

Gasse, F. and Street, F.A., 1978. Late Quaternary Lake-level fluctuations and environments of the northern Rift valley and Afar region (Ethiopia and Djibouti). Palaeogeography, Palaeoclimatology, Palaeoecology, 24(4): 279-325.

Gibert, E., Travi, Y., Massault, M., Chernet, T., Barbecot, F. and Laggoun, D.F., 1999. Comparing carbonate and organic AMS- (super 14) C ages in Lake Abiyata sediments (Ethiopia); hydrochemistry and paleoenvironmental implications. Radiocarbon, 41(3): 271-286.

Gibert, E., Travi, Y., Massault, M., Tiercelin, J.-J. and Chernet, T., 2002. AMC-14C chronology of a lacustrine sequence from Lake Langano (Main Ethiopian Rift): Correction and validation steps in relation with volcanism, lake water and carbon balances. Radiocarbon, 44(1): 75-92.

Gibson, I.L., 1967. Preliminary account of the volcanic geology of Fantale, Shoa. Bulletin of the Geophysical Observatory, Addis Ababa, 10: 59-67.

Gibson, I.L., 1970. A pantelleritic welded ash-flow tuff from the Ethiopian Rift Valley. Contr. Mineral. and Petrol., 28(2): 89-111.

Gibson, I.L., 1974. A review of the geology, petrology and geochemistry of the volcano Fantale. Bull Volcanol, 38(2): 791-802.

Giordano, F., D'Antonio, M., Civetta, L., Tonarini, S., Orsi, G., Ayalew, D., Yirgu, G., Dell'Erba, F., Di Vito, M.A. and Isaia, R., 2014. Genesis and evolution of mafic and felsic magmas at Quaternary volcanoes within the Main Ethiopian Rift: Insights from Gedemsa and Fanta 'Ale complexes. Lithos, 188(0): 130-144.

Gouin, P., 1979. Earthquake History of Ethiopia and the Horn of Africa. 256.

Green, R.M., Bebbington, M.S., Jones, G., Cronin, S.J. and Turner, M.B., 2016. Estimation of tephra volumes from sparse and incompletely observed deposit thicknesses. Bulletin of Volcanology, 78(4): 1-18.

Harris W.C., 1844. The Highlands of Aethiopia (3 Vols, 2nd Edition). Vol III, Longman, Brown, Green and Longmans, London, 436 pp.

Hunt, J.A., Zafu, A., Mather, T.A., Pyle, D.M. and Barry, P.H., 2017. Spatially variable CO_2 degassing in the Main Ethiopian Rift: Implications for magma storage, volatile transport, and rift-related Emissions. Geochemistry, Geophysics, Geosystems, 18(10): 3714-3737.

Hutchison, W., Biggs, J., Mather, T.A., Pyle, D.M., Lewi, E., Yirgu, G., Caliro, S., Chiodini, G., Clor, L.E. and Fischer, T.P., 2016. Causes of unrest at silicic calderas in the East African Rift: New constraints from InSAR and soil-gas chemistry at Aluto volcano, Ethiopia. Geochemistry, Geophysics, Geosystems, 17: n/a-n/a.

Hutchison, W., Fusillo, R., Pyle, D.M., Mather, T.A., Blundy, J.D., Biggs, J., Yirgu, G., Cohen,

B.E., Brooker, R.A., Barfod, D.N. and Calvert, A.T., 2016. A pulse of mid-Pleistocene rift volcanism in Ethiopia at the dawn of modern humans. Nature Communications, 7: 13192.

Hutchison, W., Mather, T.A., Pyle, D.M., Biggs, J. and Yirgu, G., 2015. Structural controls on fluid pathways in an active rift system: A case study of the Aluto volcanic complex. Geosphere.

Hutchison, W., Pyle, D.M., Mather, T.A., Yirgu, G., Biggs, J., Cohen, B.E., Barfod, D.N. and Lewi, E., 2016. The eruptive history and magmatic evolution of Aluto volcano: new insights into silicic peralkaline volcanism in the Ethiopian rift. Journal of Volcanology and Geothermal Research, 328: 9-33.

Jeffery, A.J., Gertisser, R., O'Driscoll, B., Pacheco, J.M., Whitley, S., Pimentel, A. and Self, S., 2016. Temporal evolution of a post-caldera, mildly peralkaline magmatic system: Furnas volcano, São Miguel, Azores. Contr. Mineral. and Petrol., 171(5): 42.

JICA, 2012. The Study on Groundwater Resources Assessment in the Rift Valley Lakes Basin in the Federal Democratic Republic of Ethiopia. Japan International Cooperation Agency, Kokusai Kogyo Co. Ltd. and Ministry of Water and Energy (MoWE), The Federal Democratic Republic of Ethiopia. Final Report (Supporting Report and Data Book), 95pp and 25 pp.

Jochum, K.P., Stoll, B., Herwig, K., Willbold, M., Hofmann, A.W., Amini, M., Aarburg, S., Abouchami, W., Hellebrand, E., Mocek, B., Raczek, I., Stracke, A., Alard, O., Bouman, C., Becker, S., Dücking, M., Brätz, H., Klemd, R., de Bruin, D., Canil, D., Cornell, D., de Hoog, C.-J., Dalpé, C., Danyushevsky, L., Eisenhauer, A., Gao, Y., Snow, J.E., Groschopf, N., Günther, D., Latkoczy, C., Guillong, M., Hauri, E.H., Höfer, H.E., Lahaye, Y., Horz, K., Jacob, D.E., Kasemann, S.A., Kent, A.J.R., Ludwig, T., Zack, T., Mason, P.R.D., Meixner, A., Rosner, M., Misawa, K., Nash, B.P., Pfänder, J., Premo, W.R., Sun, W.D., Tiepolo, M., Vannucci, R., Vennemann, T., Wayne, D. and Woodhead, J.D., 2006. MPI-DING reference glasses for in situ microanalysis: New reference values for element concentrations and isotope ratios. Geochem. Geophys. Geosyst., 7(2): Q02008.

Jochum, K.P., Weis, U., Stoll, B., Kuzmin, D., Yang, Q., Raczek, I., Jacob, D.E., Stracke, A.,

Birbaum, K., Frick, D.A., Günther, D. and Enzweiler, J., 2011. Determination of Reference Values for NIST SRM 610–617 Glasses Following ISO Guidelines. Geostandards and Geoanalytical Research, 35(4): 397-429.

Keir, D., Bastow, I.D., Corti, G., Mazzarini, F. and Rooney, T.O., 2015. The origin of along-rift variations in faulting and magmatism in the Ethiopian Rift. Tectonics, 34(3): 464-477.

Keir, D., Stuart, G.W., Jackson, A. and Ayele, A., 2006. Local Earthquake Magnitude Scale and Seismicity Rate for the Ethiopian Rift. Bulletin of the Seismological Society of America, 96(6): 2221-2230.

Kendall, J.-M., Stuart, G.W., Ebinger, C.J., Bastow, I.D., Keir, D., 2005. Magma-assisted rifting in Ethiopia. Nature, 433: 146 - 148.

Keranen, K., Klemperer, S.L., Gloaguen, R. and Group, E.W., 2004. Three-dimensional seismic imaging of a protoridge axis in the Main Ethiopian rift. Geology, 32(11): 949-952.

Keynes, S., 2007 (ed). Ethiopian encounters: Sir William Cornwallis Harris and the British Mission to the Kingdom of Shewa (1841-3). Fitzwilliam Museum, Cambridge, 72 pp.

Le Bas, M.J., LeMaitre, R.W., Streckheisen, A., Zanettin, B., 1986. Chemical classification of volcanic rocks based on the total alkali–silica diagram. Journal of Petrology 27, 745–750.

Le Turdu, C., Tiercelin, J.-J., Gibert, E., Travi, Y., Lezzar, K.-E., Richert, J.-P., Massault, M., Gasse, F., Bonnefille, R., Decobert, M., Gensous, B., Jeudy, V., Tamrat, E., Mohammed, M.U., Martens, K., Atnafu, B., Chernet, T., Williamson, D. and Taieb, M., 1999. The Ziway–Shala lake basin system, Main Ethiopian Rift: Influence of volcanism, tectonics, and climatic forcing on basin formation and sedimentation. Palaeogeography, Palaeoclimatology, Palaeoecology, 150(3–4): 135-177.

Leat, P.T., 1984. Geological evolution of the trachytic caldera volcano Menengai, Kenya Rift Valley. Journal of The Geological Society of London, 141: 1057-1069.

Lézine, A.-M., Ivory, S.J., Braconnot, P. and Marti, O., 2017. Timing of the southward retreat of the ITCZ at the end of the Holocene Humid Period in Southern Arabia: Data-model comparison. Quaternary Science Reviews, 164: 68-76.

MacDonald, R., 1974. Nomenclature and petrochemistry of the peralkaline oversaturated

extrusive rocks. Bulletin Volcanologique, 38(2): 498-516.

Macdonald, R., Bagiński, B., Ronga, F., Dzierżanowski, P., Lustrino, M., Marzoli, A. and Melluso, L., 2012. Evidence for extreme fractionation of peralkaline silicic magmas, the Boseti volcanic complex, Main Ethiopian Rift. Miner Petrol, 104(3): 163-175.

Mahood, G.A., 1984. Calderas associated with strongly peralkaline volcanic rocks. Journal of Geophysical Research 89:8540–8552.

Mahood, G.A. and Hildreth, W., 1986. Geology of the peralkaline volcano at Pantelleria, Strait of Sicily. Bulletin of Volcanology, 48(2): 143-172.

Manville, V., Segschneider, B., Newton, E., White, J.D.L., Houghton, B.F. and Wilson, C.J.N., 2009. Environmental impact of the 1.8 ka Taupo eruption, New Zealand: Landscape responses to a large-scale explosive rhyolite eruption. Sedimentary Geology, 220(3): 318-336.Martin-Jones, C.M., Lane, C.S., Pearce, N.J., Smith, V.C., Lamb, H.F., Schaebitz, F., Viehberg, F., Brown, M.C., Frank, U. and Asrat, A., 2017. Recurrent explosive eruptions from a high-risk Main Ethiopian Rift volcano throughout the Holocene. Geology, 45(12): 1127-1130.

Mengistu Darge, Y., Tesfaw Hailu, B., Atnafu Muluneh, A., Kidane, T., 2017. Detection of geothermal anomalies using Landsat 8 TIRS data in Tulu Moye geothermal prospect, Main Ethiopian Rift. The 4th National GIS Summit, 13-15 January 2017, Bahir Dar University, Ethiopia.

Meyer, W., Pilger, A., Rosler, A., Stets, J., 1975. Tectonic evolution of the northern part of the Main Ethiopian Rift in Southern Ethiopia. In: Pilger, A., Rosler, A. (eds) *Afar Depression of Ethiopia.* Schweizerbart, Stuttgart, pp. 352–362.

Mohr, P., 1962. The Ethiopian Rift System. Bulletin of the Geophysical Observatory, Addis Ababa, 3(1): 33-62.

Mohr, P., Mitchell, J.G. and Raynolds, R.G.H., 1980. Quaternary volcanism and faulting at O'A caldera, central ethiopian rift. Bull Volcanol, 43(1): 173-189.

Mohr, P.A., 1966. Chabbi volcano (ethiopia). Bull Volcanol, 29(1): 797-815.

Mohr, P.A. and Wood, C.A., 1976. Volcano spacings and lithospheric attenuation in the Eastern Rift of Africa. Earth and Planetary Science Letters, 33(1): 126-144.

Morton, W.H., Rex, D.C., Mitchell, J.G. and Mohr, P., 1979. Riftward younging of volcanic units in the Addis Ababa region, Ethiopian rift valley. Nature, 280(5720): 284-288.

Neave, D.A., Fabbro, G., Herd, R.A., Petrone, C.M. and Edmonds, M., 2012. Melting, Differentiation and Degassing at the Pantelleria Volcano, Italy. Journal of Petrology, 53(3): 637-663.

Negash, A., Alene, M., Brown, F.H., Nash, B.P. and Shackley, M.S., 2007. Geochemical sources for the terminal Pleistocene/early Holocene obsidian artifacts of the site of Beseka, central Ethiopia. Journal of Archaeological Science, 34(8): 1205-1210.

Newhall, C.G., Dzurisin, D., 1988. Historical unrest at large calderas of the world, 1108 pp.

Newhall, C.G., Self, S., 1982. The Volcanic Explosivity Index (VEI) - An estimate of explosive magnitude for historical volcanism. Journal of Geophysical Research, 87(C2): 1231-1238.

Orsi, G., Ruvo, L. and Scarpati, C., 1991. The recent explosive volcanism at Pantelleria. Geologische Rundschau, 80(1): 187-200.

Pearce, N.J.G., Abbott, P.M. and Martin-Jones, C., 2014. Microbeam methods for the analysis of glass in fine-grained tephra deposits: a SMART perspective on current and future trends. Geological Society, London, Special Publications, 398(1): 29-46.

Peccerillo, A., Barberio, M.R., Yirgu, G., Ayalew, D., Barbieri, M. and Wu, T.W., 2003. Relationships between Mafic and Peralkaline Silicic Magmatism in Continental Rift Settings: a Petrological, Geochemical and Isotopic Study of the Gedemsa Volcano, Central Ethiopian Rift. Journal of Petrology, 44(11): 2003-2032.

Poppe, S., Smets, B., Fontijn, K., Rukeza, M.B., De Marie Fikiri Migabo, A., Milungu, A.K., Namogo, D.B., Kervyn, F. and Kervyn, M., 2016. Holocene phreatomagmatic eruptions alongside the densely populated northern shoreline of Lake Kivu, East African Rift: timing and hazard implications. Bulletin of Volcanology, 78(11): 82.

Pyle, D.M., 1989. The thickness, volume and grainsize of tephra fall deposits. Bulletin of Volcanology, 51(1): 1-15.

Pyle, D.M., 1999. Widely dispersed Quaternary tephra in Africa. Global and Planetary Change, 21(1–3): 95-112.

Pyle, D.M., 2015. Sizes of Volcanic Eruptions. Encyclopedia of Volcanoes, 2: 257-264.

Pyle, D.M., 2016. Field observations of tephra fallout deposits. In: Mackie, S., Cashman, K., Ricketts, H., Rust, A., Watson, M. (eds) *Volcanic Ash. Hazard Observation*. Elsevier, p25–38.

Rampey, M.L., Oppenheimer, C., Pyle, D.M. and Yirgu, G., 2010. Caldera-forming eruptions of the Quaternary Kone Volcanic Complex, Ethiopia. Journal of African Earth Sciences, 58(1): 51-66.

Rapprich, V., Čížek, D., Daniel, K., Firdawok, L., Habtamu, B., Hroch, T., Kopačková, V.,Málek, J., Malík, J., Mišurec, J., Orgoň, A., Šebesta, J., Šíma, J., Tsigehana, T., Verner, K., Yewubinesh, B., 2013. Explanation Booklet to the Set of Geosciencemaps of Ethiopia at scale 1:50,000, subsheet 0738-C4 Hawasa. Czech Geological Survey / Aquatest / Geological Survey of Ethiopia, Praha / Addis Ababa, Czech Republic / Ethiopia, pp. 1–46

Rapprich, V., Žáček, V., Verner, K., Erban, V., Goslar, T., Bekele, Y., Legesa, F., Hroch, T. and Hejtmánková, P., 2016. Wendo Koshe Pumice: The latest Holocene silicic explosive eruption product of the Corbetti Volcanic System (Southern Ethiopia). Journal of Volcanology and Geothermal Research, 310: 159-171.

Rawson, H., Naranjo, J.A., Smith, V.C., Fontijn, K., Pyle, D.M., Mather, T.A. and Moreno, H., 2015. The frequency and magnitude of post-glacial explosive eruptions at Volcán Mocho-Choshuenco, southern Chile. Journal of Volcanology and Geothermal Research, 299(0): 103-129.

Reimer, P.J., Bard, E., Bayliss, A., Beck, J.W., Blackwell, P.G., Bronk Ramsey, C., Buck, C.E., Cheng, H., Edwards, R.L., Friedrich, M., Grootes, P.M., Guilderson, T.P., Haflidason, H., Hajdas, I., Hatté, C., Heaton, T.J., Hoffmann, D.L., Hogg, A.G., Hughen, K.A., Kaiser, K.F., Kromer, B., Manning, S.W., Niu, M., Reimer, R.W., Richards, D.A., Scott, E.M., Southon, J.R., Staff, R.A., Turney, C.S.M. and van der Plicht, J., 2013. IntCal13 and Marine13 radiocarbon age calibration curves 0-50,000 years cal BP. Radiocarbon, 55(4): 1869-1887.

Robertson, E., Biggs, J., Edmonds, M., Clor, L., Fischer, T.P., Vye-Brown, C., Kianji, G., Koros, W. and Kandie, R., Diffuse degassing at Longonot volcano, Kenya: Implications for

CO2 flux in continental rifts. Journal of Volcanology and Geothermal Research.

Ronga, F., Lustrino, M., Marzoli, A. and Melluso, L., 2010. Petrogenesis of a basalt-comendite-pantellerite rock suite: the Boseti Volcanic Complex (Main Ethiopian Rift). Miner Petrol, 98(1-4): 227-243.

Rooney, T., Furman, T., Bastow, I., Ayalew, D. and Yirgu, G., 2007. Lithospheric modification during crustal extension in the Main Ethiopian Rift. Journal of Geophysical Research: Solid Earth, 112(B10): n/a-n/a.

Rooney, T.O., Bastow, I.D., Keir, D., 2011. Insights into extensional processes during magma assisted rifting: Evidence from aligned scoria cones. Journal of Volcanology and Geothermal Research, 201: 83-96.

Rooney, T.O., Furman, T., Yirgu, G. and Ayalew, D., 2005. Structure of the Ethiopian lithosphere: Xenolith evidence in the Main Ethiopian Rift. Geochimica et Cosmochimica Acta, 69(15): 3889-3910.

Scott, S.C., 1980. The Geology of Longonot Volcano, Central Kenya: A Question of Volumes. Philosophical Transactions of the Royal Society of London: Mathematical and Physical Sciences, 296(1420): 437-465.

Siebert, L., Simkin, T. and Kimberly, P., 2010. Volcanoes of the World - Third Edition. University of California Press, Berkeley, 568 pp.

Siegburg, M., Gernon, T.M., Bull, J.M., Keir, D., Barfod, D.N., Taylor, R.N., Abebe, B., Ayele, A., 2018. Geological evolution of the Boset-Bericha Volcanic Complex, Main Ethiopian Rift: ^{40}Ar/^{39}Ar evidence for episodic Pleistocene to Holocene volcanism. Journal of Volcanology and Geothermal Research, https://doi.org/10.1016/j.jvolgeores.2017.12.014

Thrall, R., 1973. Gadamsa Caldera, Ethiopia. Centre for Astrophysics, Dartmouth College, Reprint Series, 280: 71-80.

Tiercelin, J.J., Gibert, E., Umer, M., Bonnefille, R., Disnar, J.R., Lézine, A.M., Hureau-Mazaudier, D., Travi, Y., Keravis, D. and Lamb, H.F., 2008. High-resolution sedimentary record of the last deglaciation from a high-altitude lake in Ethiopia. Quaternary Science Reviews, 27(5–6): 449-467.

Trua, T., Deniel, C. and Mazzuoli, R., 1999. Crustal control in the genesis of Plio-Quaternary bimodal magmatism of the Main Ethiopian Rift (MER): geochemical and isotopic (Sr, Nd, Pb) evidence. Chemical Geology, 155(3–4): 201-231.

USAID (2017) Power Africa Programme; http://www.usaid.gov/powerafrica; accessed June 2017.

Vogel, N., Nomade, S., Negash, A. and Renne, P.R., 2006. Forensic 40Ar/39Ar dating: a provenance study of Middle Stone Age obsidian artifacts from Ethiopia. Journal of Archaeological Science, 33(12): 1749-1765.

Wadge, G., Biggs, J., Lloyd, R. and Kendall, J.-M., 2016. Historical Volcanism and the State of Stress in the East African Rift System. Frontiers in Earth Science, 4(86).

Wauthier, C., Cayol, V., Poland, M., Kervyn, F., d'Oreye, N., Hooper, A., Samsonov, S., Tiampo, K. and Smets, B., 2013. Nyamulagira's magma plumbing system inferred from 15 years of InSAR. Geological Society, London, Special Publications, 380(1): 39-65.

White, J.D.L. and Valentine, G.A., 2016. Magmatic versus phreatomagmatic fragmentation: Absence of evidence is not evidence of absence. Geosphere, 12(5).

Wilks, M., Kendall, J.M., Nowacki, A., Biggs, J., Wookey, J., Birhanu, Y., Ayele, A. and Bedada, T., 2017. Seismicity associated with magmatism, faulting and hydrothermal circulation at Aluto Volcano, Main Ethiopian Rift. Journal of Volcanology and Geothermal Research 340: 52-67

Williams, F.M., Williams, M.A.J. and Aumento, F., 2004. Tensional fissures and crustal extension rates in the northern part of the Main Ethiopian Rift. Journal of African Earth Sciences, 38(2): 183-197.

Wilson, T., Stewart, C., Sword-Daniels, V., Leonard, G., Johnston, D., Cole, J., Wardman, J., Wilson, G., Barnard, S., 2012. Volcanic ash impacts on critical infrastructure. Physics and Chemistry of the Earth, 45-45: 5-23.

WoldeGabriel, G., Aronson, J.L. and Walter, R.C., 1990. Geology, geochronology, and rift basin development in the central sector of the Main Ethiopia Rift. Geological Society of America Bulletin, 102(4): 439-458.

Wolfenden, E., Ebinger, C., Yirgu, G., Deino, A., Ayalew, D., 2004. Evolution of the northern Main Ethiopian Rift: Birth of a Triple Junction. Earth and Planetary Science Letters, 224: 213 - 228.

Figures

Fig 1 Overview of Main Ethiopian Rift with Late Pleistocene – Holocene active volcanic centres, small eruptive centres and main tectonic features. Outcrops visited (yellow dots) span most of the MER; lake sediment cores with described tephra horizons indicated in blue. For clarity, the Wonji Faults are not drawn; they largely control the spatial distribution of basaltic small eruptive centres along the rift axis.

Fig 2 Isopach map of Wendo Koshe Younger Pumice (WKYP, turquoise) deposit from Corbetti as identified from lateral tracing in the field and geochemical analysis. Thicknesses of individual measurements in cm; contours are drawn tentatively where dispersal is poorly constrained. Thickness values for Bedded Pumice (in orange) are also given in cm but no contours are drawn. Reference sites for stratigraphy (named MER- and 3-digit number) are schematically illustrated in Fig 3. Caldera wall and post-caldera edifices are also outlined (A: Artu, U: Urji, C: Chabbi). Extra-caldera small eruptive centres (SECs) to the east of Lake Hawassa are basaltic and possibly phreatomagmatic in origin (Rapprich et al. 2013). A rhyolitic tuff complex immediately north of the lake is onlapped by Chabbi obsidian flows and may also be phreatomagmatic. Other SECs, in the form of magmatic scoria cones, occur north of Corbetti along fractures extending to the Shala Caldera. Post-caldera Tullu Fike

pumice cone complex indicated north of Shala. Other extra-caldera vents north and south of the caldera, and presumably of basaltic composition, are also of unknown age.

Fig 3 Schematic representation of Corbetti's composite Holocene pyroclastic stratigraphy; locations of reference sites indicated on Fig 2. Inset shows major element analyses of distinct pyroclastic units revealing systematic pantelleritic composition. Non-correlated Corbetti units indicated as small grey dots. Names and ages of Lake Tilo (TT-) and Hawassa (AWT-) tephras after Martin-Jones et al. (2017).

Fig 4 Field photographs for reference sections of Holocene pyroclastic deposits shown in Fig 2-3 (Corbetti) and Fig 5 (Aluto); same colour coding. **(a)** Coarse pumice lapilli breccia of WKYP covering finer grained Bedded Pumice; black arrow denotes ca. 10-15 cm palaeosol between deposits. **(b)** Oldest sequence of Holocene pyroclastic deposits exposed in terrestrial sections as described in this study; black arrow shows sample location of charcoal dated 7.75 ± 0.04 ka cal BP (Table 3); people for scale; **(c)** Exposure of lacustrine deposits interbedded with pyroclastic deposits (typically darker grey horizons) in type section A01 (Fig 5); **(d)** Close-up of pyroclastic deposit inferred to be emplaced under water: bottom half clast-supported pumice lapilli with some intergranular fine ash, top half pumice lapilli dispersed in more ash-rich matrix; pencil for scale

Fig 5 Spatial distribution of sample localities at Aluto, with identification of type locality A01 (stratigraphic column on right); some locally correlated deposits colour-coded as in Fig 6, with deposit thickness indicated in cm; tephra from other sites (grey dots) did not yield correlations across multiple localities. Selected named outcrops also represented in Fig 4c-d, 6 and S1c-d ("MER" omitted from the 3-digit labels for clarity, "WH_" omitted from other

labels; full details in Supplementary Table 2). SEC: Small Eruptive Centre – those close and possibly associated to the Aluto complex are distinguished from the ones in East Ziway; TC: tuff cone; TAC: trachyandesitic scoria cone. High-resolution LIDAR digital elevation model on the Aluto edifice after Hutchison et al. (2015).

Fig 6 The glass major element composition of geologically young Aluto pumice samples. These span a wide range of mostly pantelleritic compositions. Some units can be correlated on a local scale, including A9 / Qup. Samples highlighted in colour are are colour-coded as in Fig 5; grey dots represent analyses of samples that could not be correlated between multiple localities. Glass chemistry for Corbetti samples (Fig 3) given for comparison, and to highlight potential correlation of sample 150207 found NE of Lake Langano (Fig 5) to Corbetti source (Fig 3). The complicated fingerprinting of Corbetti samples however requires additional verification to validate this correlation.

Fig 7 Overview map of Bora-Baricha, Tullu Moye and Gedemsa area. Both post-caldera scoria cones near Gedemsa and Tully Moye, as well as rhyolitic lava flows of Tullu Moye are controlled by the Wonji Fault Belt. SECs indicated in orange have confirmed basaltic glass composition (samples MER153A and MER157A in Supplementary Table 3a). Gedemsa caldera is outlined in dark blue, with extent of its post-caldera constructs in pink. The dotted pink lines highlight low-relief dome-shaped constructs which are presumably also post-caldera centres of activity. Dots indicate sample sites, and those at Gedemsa are colour-coded as in Figure 9. Selected outcrops from Figures 8-9 (omitting "MER-", for clarity; Supplementary Table 2) are named.

Fig 8 (a) Bora-Baricha representative field photos showing alternation of pyroclastic fall deposits and palaeosols (MER147-1/2) and a stack of multiple-metre-thick pyroclastic fall and dilute PDC deposits alternating with poorly developed soils and ash-rich reworked horizons (MER150). These deposits have not been chemically correlated to other units in the region but were most likely sourced from Bora-Baricha or associated edifices; colour-coded with (b) and (c). **(b)** Bora-Baricha and Tullu Moye key stratigraphic sections, spanning all sides of the complex (Fig 7). Many eruptions have emplaced several meters of pyroclastic fall deposits, and most sections show only limited soil formation between events. **(c)** Glass major element composition of Bora-Baricha and Tullu Moye silicic pyroclastic deposits. Bora-Borecha samples are pantelleritic whereas those of Tullu Moye are comenditic. The top unit of section MER150 has a distinct composition to the rest of the sequence and may form a fractionation trend with Tullu Moye comendites.

Fig 9 (a-c) Gedemsa representative field photos: **(a)** MER084, crudely bedded dark grey pumice lapilli breccia alternating with low-angle cross-bedded fine pumice and ash lapilli deposits, presumably related to caldera-forming events, and chemically correlated to MER077; scraper (encircled in yellow) for scale. **(b)** MER087: poorly sorted pumice lapilli and bomb breccia exposed on rim of Kore crater, the most prominent post-caldera centre; pencil for scale. **(c)** MER081: (presumably) post-caldera pumice lapilli breccia deposit exposed underneath cross-bedded indurated tuff deposits associated to mafic volcanism near the NE rim of the caldera. **(d-e)** Gedemsa glass geochemistry for a selection of samples obtained

from multiple syn-caldera pumice breccia deposits and post-caldera pumice deposits (colour-coded as in Fig 7). The three most FeO-rich deposits originate from the intra-caldera coalesced domes Kelo, Dima and Kore. Three more chemically distinct pumice fall deposits are identified and were sampled from sections immediately NE and E of the caldera. Each of these presumably represents an individual moderately explosive post-caldera eruption. The age of these post-caldera events is not known.

Fig 10 Overview map of Boset volcanic complex, with overlain isopach map (thickness in cm) of the Boset Pumice deposit. Tephra was mainly dispersed westward, with accumulations multiple metres thick on the lower western flanks of the complex. The dispersal towards the north and east is poorly constrained; however none of the outcrops in those regions revealed the presence of substantial pumice fall deposits. Named outcrops are those listed in Fig 11. ([1]) One lobe of trachyandesitic lava was dated at 4.2 ± 3.2 ka (Siegburg et al. 2018) and may correspond to Scoria #2 in our type section MER108 (Fig 11).

Fig 11 Glass geochemistry and type stratigraphy of the most recent pyroclastic deposits at Boset volcanic complex; **(a)** Total Alkali – Silica diagram (after Le Bas et al. 1986) showing rhyolitic pumice deposits and basaltic scoria deposits. A scoria fall deposit interbedded in the type stratigraphy (unit #2) has a basaltic trachyandesite composition and possibly corresponds to the eruption of lava flows in the saddle between Gudda and Bericha (Siegburg et al. 2018). The most evolved rhyolites are from a sequence of altered coarse grey pumice fall deposits and finely parallel to cross-bedded dilute PDC deposits, which may relate to a caldera-forming event; **(b)** Classification diagram of peralkaline rhyolites (after MacDonald 1974) shows the three most recent pumice fall units to have a pantelleritic

composition, whereas the oldest pumice fall (#5) is comenditic. There may be multiple comendite falls but more field and geochemical data are required to verify this. Mafic samples in this plot are given for reference only. **(c)** Schematic log of type stratigraphic section for recent pyroclastic deposits, colour-coded as in **(a)** and **(b)**; **(d)** Field photograph of "Boset Pumice", unit #1, in locality MER113 (Fig 10).

Fig 12 Overview map of Kone caldera complex and Fentale, with indication of basaltic scoria cones which erupted as recently as 1810-1820 AD (Harris 1844; Supplementary Table 1). Fentale has experienced post-caldera silicic volcanism in the form of obsidian lava flows erupted from vents in the caldera floor and on the NE, E, SE and W flanks. At Kone there is no evidence for post-caldera silicic volcanism.

Fig 13 Glass chemical composition of a selection of scoria fall deposits and pumice lapilli breccia associated to caldera-forming events at the Kone caldera complex. Corresponding map units of Rampey et al. (2010) indicated in brackets. Glass composition of obsidian source rocks from Kone after Negash et al. (2007).

Tables

Table 1 Average glass major element composition of main units at each volcanic centre (full dataset in Supplementary Table 3a)

Table 2 Synoptic summary of MER post-caldera silcic and mafic eruptive activity, as constrained by edifice morphology, field observations, geochemistry, geochronology and previously published literature. Items for which no information is available have been left blank. PDC: pyroclastic density current.

Table 3 New Accelerator Mass Spectroscopy radiocarbon date for charcoal sample buried under Corbetti pyroclastic fall deposit. Analysis was performed at Beta Analytic Inc., Florida, USA. Ages are reported as years before present (yr BP), "present" being 1950 CE, as per international convention. Calibration was performed in Oxcal v4.3 using the IntCal13 calibration curve (http://c14.arch.ox.ac.uk; Bronk Ramsey 2009; Reimer et al. 2013).

Table 1 Average glass major element composition of main units at each volcanic centre (full dataset in Supplementary Table 3a)

Volcano	Corbetti								Aluto - Type Section A01												Aluto			
Unit / Sample	WKYP		Bedded Pumice		MER010C		MER010J		Qup		A01_A8		A01_A7		A01_A6		A01_A5		MER053 A/B		170101K		310112A	
n samples	5		12		1		1		7		7		2		2		3		4		1		1	
	n=9		n=28		n=2		n=2		n=1		n=1		n=4		n=4		n=5		n=8		n=2		n=2	
wt%	2	SD	9	SD	3	SD	2	SD	53	SD	43	SD	8	SD	1	SD	1	SD	8	SD	8	SD	3	SD
SiO_2	75.14	0.22	75.20	0.29	75.41	0.15	74.97	0.20	73.40	0.42	74.08	0.33	73.67	0.47	73.27	0.44	73.21	0.49	74.39	0.41	75.54	0.62	71.41	0.27
TiO_2	0.26	0.03	0.26	0.03	0.25	0.03	0.21	0.03	0.18	0.04	0.19	0.05	0.31	0.04	0.34	0.04	0.32	0.04	0.24	0.03	0.18	0.03	0.41	0.03
Al_2O_3	9.52	0.17	9.55	0.18	9.80	0.12	9.42	0.07	8.13	0.27	8.82	0.21	9.84	0.27	8.88	0.18	8.89	0.42	9.14	0.13	11.00	0.20	10.45	0.11
FeO^T	4.59	0.16	4.60	0.24	4.76	0.13	4.87	0.13	6.65	0.23	5.76	0.21	5.23	0.17	6.48	0.22	6.44	0.34	5.39	0.17	3.31	0.25	6.17	0.17
MnO	0.22	0.05	0.21	0.04	0.22	0.04	0.23	0.04	0.32	0.05	0.26	0.04	0.22	0.04	0.31	0.05	0.31	0.05	0.23	0.05	0.15	0.04	0.28	0.04
MgO	0.01	0.01	0.01	0.01	0.00	0.01	0.00	0.01	0.01	0.01	0.01	0.01	0.02	0.02	0.02	0.02	0.02	0.02	0.01	0.01	0.01	0.01	0.02	0.01
CaO	0.19	0.03	0.19	0.02	0.19	0.02	0.18	0.02	0.20	0.04	0.20	0.03	0.26	0.03	0.27	0.03	0.27	0.03	0.21	0.03	0.18	0.04	0.37	0.03
Na_2O	5.54	0.17	5.40	0.26	4.85	0.22	5.67	0.16	6.70	0.55	6.29	0.26	5.96	0.18	5.96	0.42	6.04	0.51	5.94	0.32	3.73	0.56	6.14	0.25
K_2O	4.53	0.09	4.58	0.10	4.51	0.09	4.43	0.07	4.39	0.15	4.38	0.11	4.48	0.12	4.46	0.13	4.48	0.11	4.43	0.10	5.89	0.24	4.73	0.21
P_2O_5	0.01	0.01	0.01	0.01	0.01	0.01	0.01	0.01	0.01	0.02	0.01	0.01	0.01	0.02	0.02	0.02	0.02	0.02	0.02	0.02	0.01	0.01	0.02	0.02
Cl	0.19	0.02	0.19	0.02	0.21	0.01	0.23	0.02	0.29	0.05	0.25	0.03	0.18	0.02	0.17	0.02	0.17	0.02	0.21	0.02	0.22	0.02	0.14	0.02

Tot	95.68	1.09	96.54	1.23	95.51	0.86	95.95	0.97	95.48	1.72	94.00	1.58	93.29	0.70	93.46	1.11	92.94	1.30	93.23	1.43	93.24	0.64	93.74	0.34

Volcano	Bora-Baricha				Tullu Moye				Gedemsa - Caldera				Gedemsa - Post-Caldera				Gedemsa - Post-Caldera?			
Unit / Sample	MER147-2A/C		MER150F		MER150C		MER152A		Cluster #1 (76AB/94A)		Cluster #2 (77B/80A/84A)		Kore		Dima (88A-C)		MER093A		MER081A	
n samples	3		1		2		2		3		3		1		3		1		1	
wt%	n=77	SD	n=30	SD	n=52	SD	n=56	SD	n=82	SD	n=71	SD	n=22	SD	n=82	SD	n=25	SD	n=19	SD
SiO$_2$	74.35	0.35	74.61	0.21	73.34	0.21	72.03	0.50	74.32	0.19	74.51	0.42	73.51	0.24	72.40	0.51	74.63	0.20	73.92	0.19
TiO$_2$	0.21	0.03	0.31	0.03	0.35	0.03	0.25	0.03	0.26	0.03	0.30	0.05	0.18	0.03	0.17	0.03	0.26	0.03	0.18	0.03
Al$_2$O$_3$	8.82	0.31	9.52	0.10	10.64	0.15	13.32	0.55	8.83	0.19	9.22	0.20	7.69	0.25	6.43	0.15	10.26	0.18	8.21	0.18
FeO^T	5.93	0.30	5.22	0.18	4.96	0.15	3.16	0.31	5.82	0.13	5.54	0.16	7.41	0.26	7.99	0.21	4.33	0.12	6.53	0.13
MnO	0.24	0.04	0.18	0.04	0.20	0.04	0.15	0.04	0.20	0.04	0.20	0.04	0.30	0.06	0.39	0.04	0.15	0.04	0.28	0.04
MgO	0.01	0.01	0.01	0.01	0.01	0.01	0.09	0.03	0.01	0.01	0.01	0.01	0.00	0.01	0.01	0.01	0.01	0.01	0.01	0.01
CaO	0.19	0.02	0.22	0.02	0.30	0.03	0.42	0.07	0.23	0.03	0.23	0.03	0.21	0.03	0.14	0.02	0.21	0.02	0.22	0.02
Na$_2$O	5.76	0.25	5.48	0.18	5.57	0.18	5.83	0.19	5.87	0.22	5.05	0.81	5.91	0.70	8.29	0.81	5.18	0.39	6.38	0.31
K$_2$O	4.49	0.10	4.43	0.08	4.62	0.13	4.74	0.11	4.46	0.13	4.93	0.56	4.78	0.62	4.16	0.33	4.95	0.47	4.26	0.13

Table continued (sample column headers appear on the preceding page):

wt%																				
P₂O₅	**0.01**	*0.01*	**0.01**	*0.02*	**0.01**	*0.01*	**0.02**	*0.02*	**0.01**	*0.01*	**0.01**	*0.01*	**0.01**	*0.01*	**0.02**	*0.01*	**0.01**	*0.01*	**0.01**	*0.01*
Cl	**0.29**	*0.02*	**0.40**	*0.01*	**0.13**	*0.02*	**0.14**	*0.02*	**0.22**	*0.02*	**0.17**	*0.02*	**0.37**	*0.02*	**0.63**	*0.03*	**0.19**	*0.02*	**0.24**	*0.01*
Tot	**94.93**	*0.78*	**94.99**	*0.56*	**94.63**	*0.89*	**95.98**	*1.69*	**94.00**	*0.57*	**93.70**	*1.02*	**93.08**	*0.70*	**95.50**	*1.75*	**94.19**	*0.52*	**92.91**	*0.46*

Volcano	Boset-Bericha						Kone			Scoria Cones (Wonji Fault Belt)				
Unit / Sample	Boset Pumice	Scoria #2	Pumice #3	Pumice #4	Comendite #5	Comendite #6	MER130A (Qpk? Qrd?)	Qpk	MER141A (Qpk? Qpb?)	East Ziway (MER068B)	Tullu Moye (MER153A)	Melkassa (MER109A)	Bericha (MER117A)	Kone (MER137A)
n samples	14	2	1	2	1	1	1	3	1	1	1	1	1	1
wt% (n=)	n=306	n=60	n=18	n=56	n=20	n=27	n=26	n=68	n=24	n=22	n=20	n=27	n=28	n=29
SiO₂	**71.39** *0.51*	**52.03** *0.49*	**72.13** *0.24*	**72.97** *0.25*	**71.76** *0.24*	**71.15** *0.22*	**73.18** *0.46*	**75.83** *0.33*	**70.19** *0.37*	**49.89** *0.70*	**50.00** *0.35*	**48.55** *0.25*	**48.05** *0.31*	**47.73** *0.24*
TiO₂	**0.30** *0.04*	**3.02** *1.0*	**0.28** *0.04*	**0.17** *0.03*	**0.29** *0.03*	**0.30** *0.04*	**0.19** *0.05*	**0.21** *0.04*	**0.48** *0.04*	**3.11** *0.14*	**3.34** *0.11*	**3.33** *0.14*	**3.18** *0.08*	**2.89** *0.07*
Al₂O₃	**8.46** *0.28*	**14.69** *0.15*	**8.04** *0.27*	**8.11** *0.13*	**13.30** *0.10*	**13.90** *0.04*	**7.98** *0.33*	**9.87** *0.19*	**9.94** *0.26*	**13.92** *0.27*	**13.55** *0.29*	**13.41** *0.34*	**13.74** *0.21*	**13.57** *0.23*
FeOᵀ	**7.67** *0.22*	**11.1** *0.3*	**7.67** *0.2*	**7.00** *0.11*	**3.18** *0.10*	**2.86** *0.09*	**6.42** *0.4*	**3.74** *0.1*	**7.14** *0.3*	**11.6** *0.7*	**13.3** *0.28*	**12.9** *0.42*	**12.9** *0.28*	**12.5** *0.27*

	1	2	3	4	5	6	7	8	9	10	11	12	13	14
	3	1	5	8		3	8	8	2	3	4	5	4	4
MnO	0.32 (0.04)	0.25 (0.04)	0.32 (0.04)	0.31 (0.05)	0.16 (0.03)	0.15 (0.03)	0.26 (0.05)	0.12 (0.05)	0.28 (0.06)	0.18 (0.04)	0.23 (0.05)	0.22 (0.03)	0.23 (0.03)	0.22 (0.07)
MgO	0.01 (0.01)	3.95 (1.6)	0.01 (0.01)	0.01 (0.01)	0.08 (0.02)	0.01 (0.02)	0.01 (0.01)	0.02 (0.02)	0.03 (0.03)	5.63 (3.7)	4.56 (0.20)	5.55 (0.30)	5.63 (0.11)	6.03 (0.11)
CaO	0.33 (0.03)	7.35 (3.2)	0.32 (0.03)	0.26 (0.02)	0.45 (0.02)	0.48 (0.02)	0.14 (0.03)	0.17 (0.03)	0.45 (0.03)	10.04 (3.6)	9.11 (0.19)	10.71 (0.38)	10.0 (0.19)	10.6 (0.19)
Na$_2$O	7.20 (0.42)	4.71 (2.5)	7.02 (2.1)	6.89 (1.5)	5.84 (0.24)	5.91 (0.17)	7.56 (4.4)	5.09 (6.6)	6.65 (5.7)	3.61 (0.83)	3.57 (0.21)	3.09 (0.32)	3.28 (0.26)	3.47 (0.21)
K$_2$O	4.29 (0.10)	1.67 (0.8)	4.21 (0.9)	4.26 (0.8)	4.92 (0.11)	5.13 (0.11)	4.25 (2.5)	4.94 (5.3)	4.82 (4.0)	1.54 (0.78)	1.37 (0.08)	1.30 (0.07)	1.19 (0.05)	1.27 (0.08)
P$_2$O$_5$	0.02 (0.01)	1.22 (0.7)	0.02 (0.02)	0.02 (0.01)	0.01 (0.01)	0.02 (0.02)	0.01 (0.02)	0.01 (0.02)	0.03 (0.02)	0.48 (0.03)	0.51 (0.03)	0.90 (0.05)	0.75 (0.04)	0.67 (0.04)
Cl	0.27 (0.02)	0.04 (0.01)	0.30 (0.02)	0.32 (0.02)	0.14 (0.02)	0.13 (0.01)				0.05 (0.02)	0.40 (0.01)	0.05 (0.01)	0.04 (0.01)	
Tot	96.42 (1.03)	97.13 (0.82)	96.67 (0.63)	96.70 (0.64)	95.84 (1.58)	93.54 (0.94)	91.28 (0.53)	91.51 (0.79)	92.38 (0.66)	96.56 (0.90)	93.70 (0.58)	97.41 (0.37)	96.85 (0.49)	94.30 (0.93)

Table 2. Synoptic summary of MER post-caldera silcic and mafic eruptive activity, as constrained by edifice morphology, field observations, geochemistry, geochronology and previously published literature. Items for which no information is available have been left blank. PDC: pyroclastic density current.

Volcanic Complex	Age of caldera-forming eruption	Earliest *dated* post-caldera activity	Post-caldera eruptive style	Deposit features	*n* events identified	Recurrence	Eruptive rate	Composition	Vent Locations	Key units	Volume / Magnitude	Thickness / Distance
Corbetti	182 ± 28 ka [1]	19 ± 15 ka [1]; 20 ± 10 ka [2]	Chabbi: obsidian lava flows with minor explosive component;	lava flows: aphyric obsidian; fall deposits: light grey aphyric pumice lapilli breccia with few % of obsidian clasts; some deposits	terrestrial: - ≥ 7 pyroclastic deposits; oldest 7.75 ka cal BP; - 12 explosive-effusive events sourced from Chabbi or Urji since Latest Pleistocene [3]	ca. 1 eruption per 700 - 1000 years	≥ 0.01 - 0.1 km^3 / ky	homogeneous aphyric pantellerite	intra-caldera; central (Urji); Eastern edge (Chabbi)			lava flows: run-out distances of 2-3 km

			Urji: dominantly explosive - tephra fall and interbedded small-scale PDC deposits (pumice cone)	rhythmically bedded at cm/dm-scale, especially in their proximal exposures; PDC deposits: stacks of subparallel to low-angle cross-bedded fine pumice and coarse ash deposits	lacustrine: - Lake Hawassa: up to 7 ash layers in ca. 7.5 ky [4] ; - Lake Tilo: up to 14 ash layers in ca. 10 ky [4]					Wendo Koshe Younger Pumice (WKYP) ~2.3 ka BP [3]; 1.3-1.9 ka cal BP [4]	V ≥ 1.3 km^3 ; ~ VEI 5	ca. 50 cm at 25 km downwind (Shashemene); elliptical dispersal
										Bedded Pumice	~ VEI 4	ca. 50 cm at 12 km; circular dispersal
			strombolian - scoria cone	scoria cones				basalt	extra-caldera: E of Lake Hawassa, N of Corbetti			
			phreatomagmatic(?)	scoria cones; tuff cone [3]	< 10 individual scoria			rhyolite; basalt [3]	SE of Chabbi; near Lake			

					cones				Hawassa			
Shala Caldera	240 ± 30 ka [5]		explosive/effusive - pumice dome		≥ 1 ?				NW of caldera	Tullu Fike	3 km³ [1]	local apron - 40 m within 2 km [5]
			strombolian - scoria cone	scoria cones	< 10 individual scoria cones			basalt	N and S of caldera			
			phreatomagmatic(?)	maar complex	≥ 1 ?			basalt?	SW of caldera			
Aluto	306 ± 12 ka; 316 ± 19 ka [1]	55 ± 19 ka [1]	tephra fall and interbedded small-scale PDC deposits erupted from pumice cones; obsidian lava flows and dome *coulées*, possibly associated with explosive phases	fall deposits: light grey crystal-poor pumice lapilli breccia with few % of obsidian clasts; some deposits crudely bedded at dm-scale; where interbedded with	terrestrial: ≥ 9 pyroclastic deposits; youngest 3 within last 7.5 ky (section A01; Fig 5) lacustrine: Lake Abijata / Langano: up to 25 ash layers in in ca. 12 ka [6-8]	ca. 2-3 eruption per 1000 years	≥ 0.01 - 0.1 km³ / ky	peralkaline rhyolite (pantellerite)	on the edifice - multiple pumice cones and domes	Qup / A9; < 7.1 ka cal BP	~VEI 3-4	3 m close to vent; 10s cm at 5 km

				lacustrine deposits, top half of deposits is typically ash-rich								
			strombolian - scoria cone					trachyandesite	NW of edifice			
			phreatomagmatic(?)	tuff cones?				basalt?	near Lake Ziway			
East Ziway			strombolian - scoria cone	scoria cones - rhythmically bedded black/red scoria lapilli and bomb breccia deposits	several tens of individual cones			basalt	East of Lake Ziway - spatially controlled by Wonji Fault Belt; separate from silicic centre of Aluto			
Bora-Baricha			Baricha: tephra fall (observed in terrestrial sequences exposed by river canyons); effusive: viscous lava flows /	light grey crystal-poor/free pumice lapilli, typically with few % of obsidian chips and dark grey	Baricha: ≥13 pumice lapilli breccia deposits alternating with soils	*limited soil formation between units*		pantellerite	Explosive: Baricha edifice?; effusive: N/NW of edifice, near Lake Koka		up to ~VEI 4/5	20 - 240 cm deposit at 4 km from the edifice

66

			dome *coulées*	pumice lapilli; crude rhythmic bedding in the biggest deposits								
			Bora(?): tephra fall; small-scale PDCs	very crystal-poor light grey coarse pumice lapilli breccia, few % obsidian chips and accidental lithics; thick packages of poorly sorted ash-supported subparallel bedded deposits with obsidian and	Bora(?): ≥ 4 units, either pumice fall or PDC deposits	*limited soil formation between units*		pantellerite	Bora SE vents?		~VEI 4-5	fall deposits up to 6 m; PDC deposits up to 7 m

				pumice clasts								
Tullu Moye	*ignimbrites exposed to SE: 115 ± 0.016 ka [9]; 1.41 ± 0.07 Ma to 1.77 ± 0.44 Ma [9]*		effusive: obsidian lava flows erupted along NE-SW fissures; explosive: tephra fall, local PDCs	lava flows: highly fractured rhyolite/obsidian flows; fall/PDC deposits: poorly sorted pumice lapilli and bomb breccias, with secondary mineralisation on the pumice lapilli and blocks of obsidian - proximal	2 comenditic pumice lapilli falls separated by soil; 1 pantelleritic pumice lapilli fall			comendite - pantellerite	fissure vents controlled by NE-SW faults	ca. 1900 AD obsidian lava flows [10]		> 5 m thick lava lobes

				fall/PDC deposits								
Gedemsa	bracketed between 265 ± 0.02 ka and 319 ± 0.02 ka [11]; 0.85 ± 0.07 Ma [12]	265 ± 0.02 ka [11]	Kelo-Dima-Kore pumice domes; tephra fall observed in soil sequences outside the caldera	intra-caldera: poorly sorted pumice lapilli and bomb breccias with obsidian clasts (proximal fall deposits); locally welded facies and interbedded obsidian lavas; extra-caldera: light grey	≥ 6 chemically unique pumice fall deposits: 3 from intra-caldera domes and 3 extra-caldera deposits			comendite - pantellerite	3 intra-caldera vents aligned WNW-ESE			extra-caldera tephra fall: up to ca. 50 cm at 5-7 km from centre of the caldera

69

				fine pumice lapilli breccia						
			strombolian - scoria cone	scoria cones - rhythmically bedded black/red scoria lapilli breccia deposits	< 10 individual scoria cones close to caldera			basalt [11]	NE - E - SE of caldera, controlled by NW-SE faults	
			phreatomagmatic (?) - dilute PDCs	subparallel and low-angle cross-bedded poorly sorted tuff deposits with up to 10-15 cm clasts of scoria, basaltic lava and				basalt? [11]	deposit exposed near NE caldera rim	

				obsidian in an ash-rich matrix								
Melkassa	*Boku caldera: 0.83 ± 0.02 Ma [12]*		strombolian - scoria cone	scoria cones	several tens of individual cones			basalt	fault-controlled; spatially separate from silicic centres of Gedemsa and Boset			
Boset (Gudda / Bericha)	Gudda caldera: < 119 ± 6 ka [13]		effusive: lava flows					trachyte - peralkaline rhyolite[13,14]	Gudda and Bericha edifices; fault-controlled			run-out distance up to 11 km [13]
								trachyandesite [15]	saddle between Gudda and Bericha [15]			run-out distance up to 13 km
			tephra fall	major units: crudely parallel bedded light grey obsidian-poor pumice lapilli	≥ 5 silicic pumice/ash falls; 1 scoria fall			comendite - pantellerite	Gudda edifice (?)	Boset Pumice	$V > 0.5$ km^3; ~ VEI 4	> 3 m at 8 km downwind; ca. 50 cm at 17 km downwind

				breccia; light grey to white pumice / coarse ash deposits; 1 black fine scoria lapilli deposit								
			strombolian - scoria cone	black / red scoria lapilli and bomb deposits with interbedded clastogenic lava flows	several tens of individual cones			basalt	mainly NE of Bericha, fault-controlled			
Kone	391 ± 2 ka; 395 ± 6 ka [16] (?)		strombolian - scoria cones, associated lava flows	a'a' lava flows; scoria fall deposits	several tens of individual cones			basalt	intra-caldera, hinge between Kone and Korke calderas; NE and SW of Kone caldera	<1808 AD(?) lava flows and scoria cone [17]		

Fentale	168 ± 38 ka [18]		silicic lava flows, possibly with minor explosive activity	obsidian/rhyolite lava flows				rhyolite	caldera floor and NE/E edifice		
			effusive	a'a lava flows	≥ 1			basalt	NE-SW fissure on S lower flank	<1808 AD(?) lava flow near Lake Beseka [17]	

References: [1] Hutchison et al. (2016c); [2] WoldeGabriel et al. (1990); [3] Rapprich et al. (2016); [4] Martin-Jones et al. (2017); [5] Mohr et al. (1980); [6] Chalié and Gasse (2002); [7] Gibert et al. (1999); [8] Gibert et al. (2002); [9] Bigazzi et al. (1993); [10] Gouin (1979); [11] Peccerillo et al. (2003); [12] Morton et al. (1979); [13] Siegburg et al. (2018); [14] Macdonald et al. (2012); [15] Brotzu et al. (1974); [16] Vogel et al. (2006); [17] Harris (1844); [18] Williams et al. (2004)

Table 3 New Accelerator Mass Spectroscopy radiocarbon date for charcoal sample buried under Corbetti pyroclastic fall deposits. Analyses were performed at Beta Analytic Inc., Florida, USA. Ages are reported as years before present (yr BP), "present" being 1950 CE, as per international convention. Calibration was performed in Oxcal v4.3 using the IntCal13 calibration curve (http://c14.arch.ox.ac.uk; Bronk Ramsey 2009; Reimer et al. 2013).

Sample ID	Lab Code	Latitude	Longitude	δ13C‰	Conventional age (^{14}C yr BP, 1 σ)	Calibrated age (cal yr BP; 95.4%)	Calibrated age mean (cal ka BP; ± 1 σ)	Sample type / Stratigraphic position
MER010K	Beta-448714	7.138 °S	38.354 °E	-25.5	6920 ± 30	7680 – 7826	7.746 ± 0.039	Charcoal in soil under Corbetti pyroclastic fall deposit
150207	Beta-465547	7.672 °S	38.811 °E	-2.9	10240 ± 40	11806 – 12136	11.966 ± 0.093	Lacustrine shells in shore deposit under pyroclastic fall deposit

Highlights

- New field and chemical data on recent volcanic activity in the Main Ethiopian Rift
- Post-caldera activity varies significantly along the rift
- Corbetti and Aluto are the most active MER volcanoes, with 1-3 events per 1000 yrs
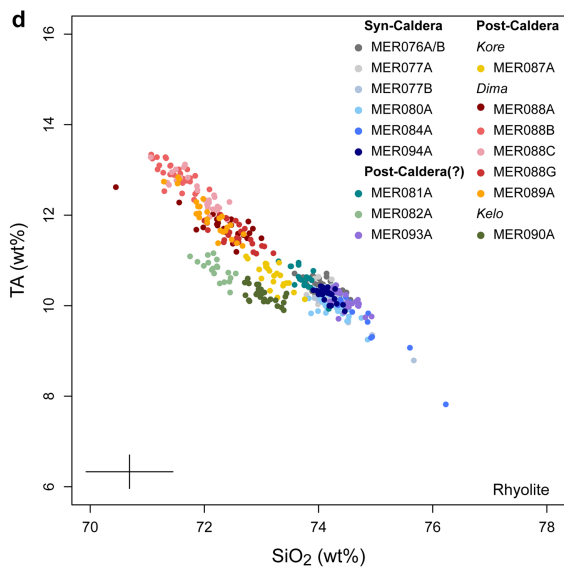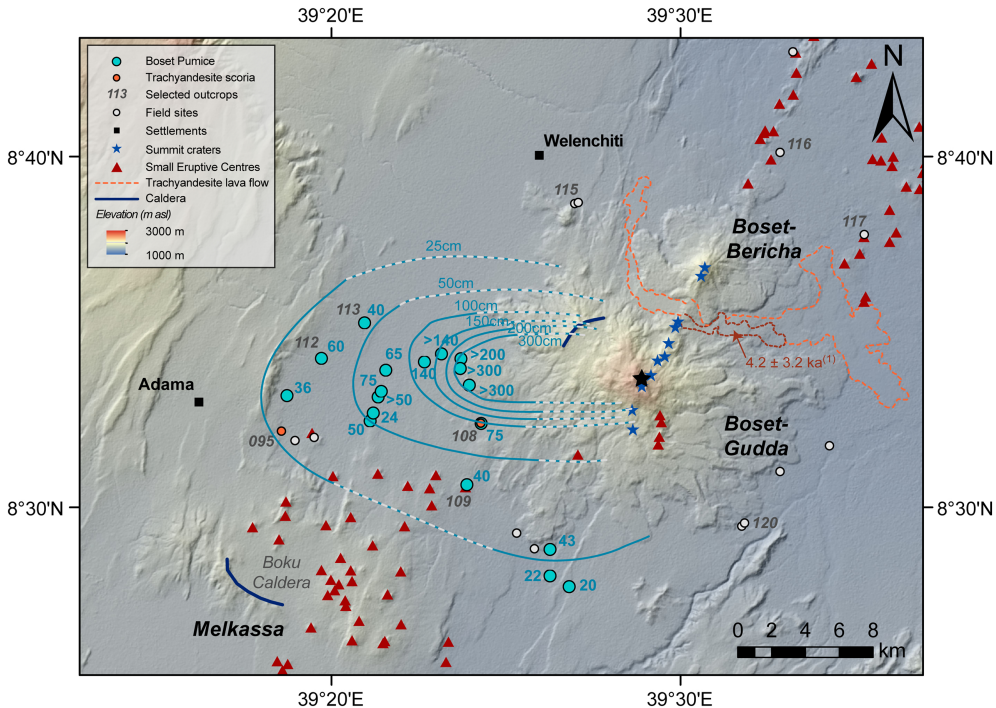- VEI 3-4 eruptions are common in the MER and often sourced from pumice cones
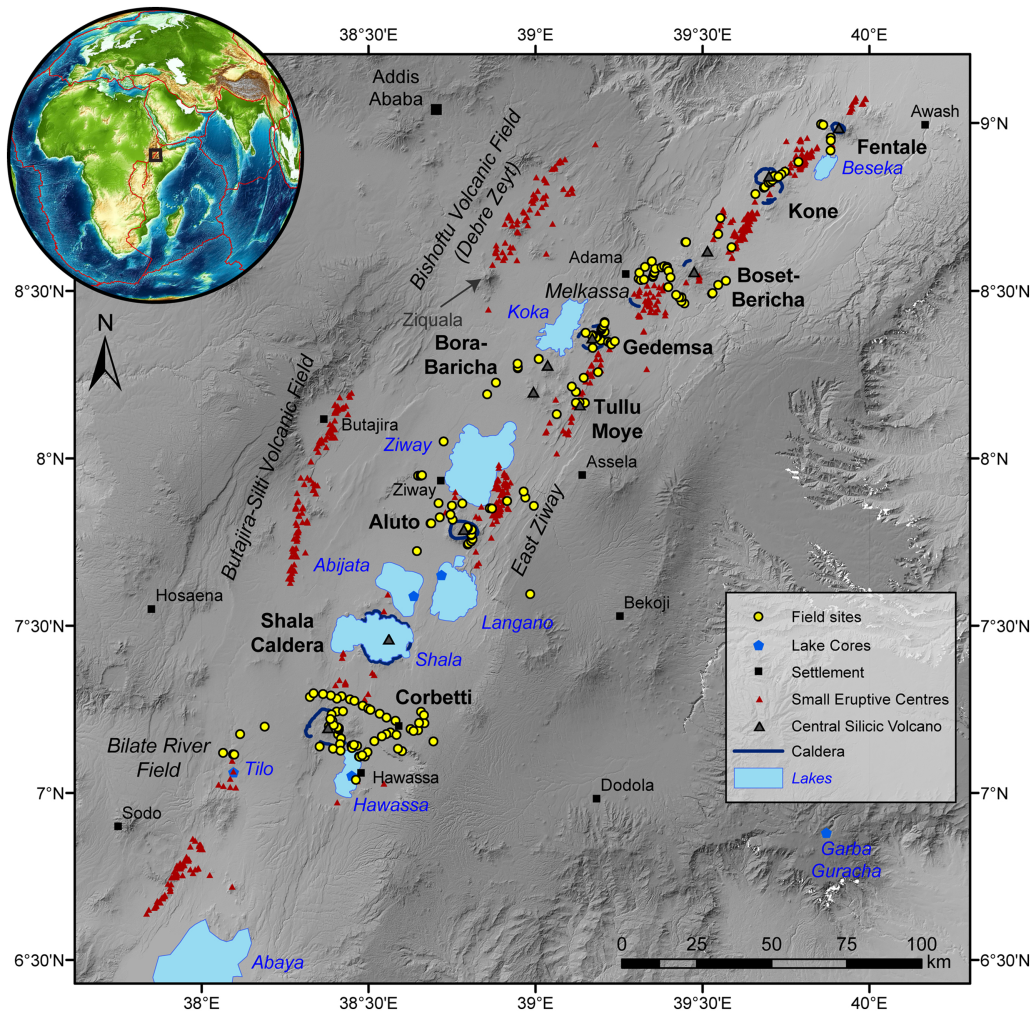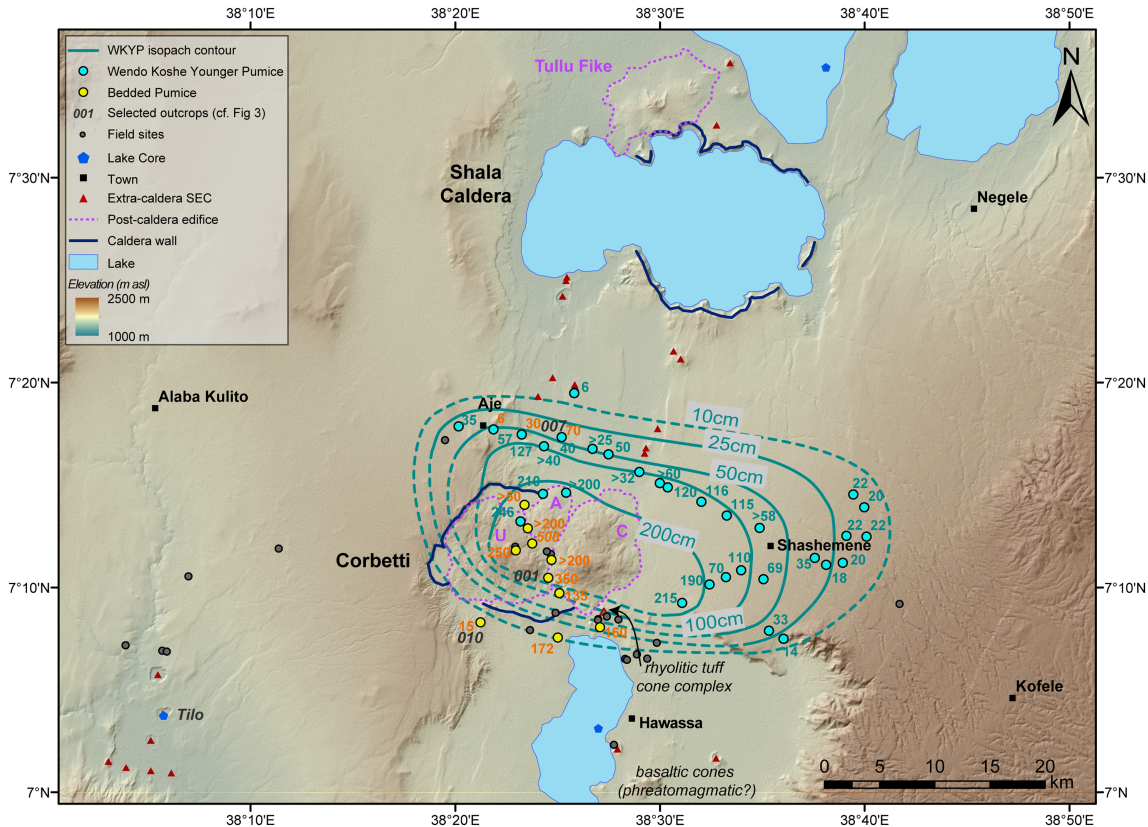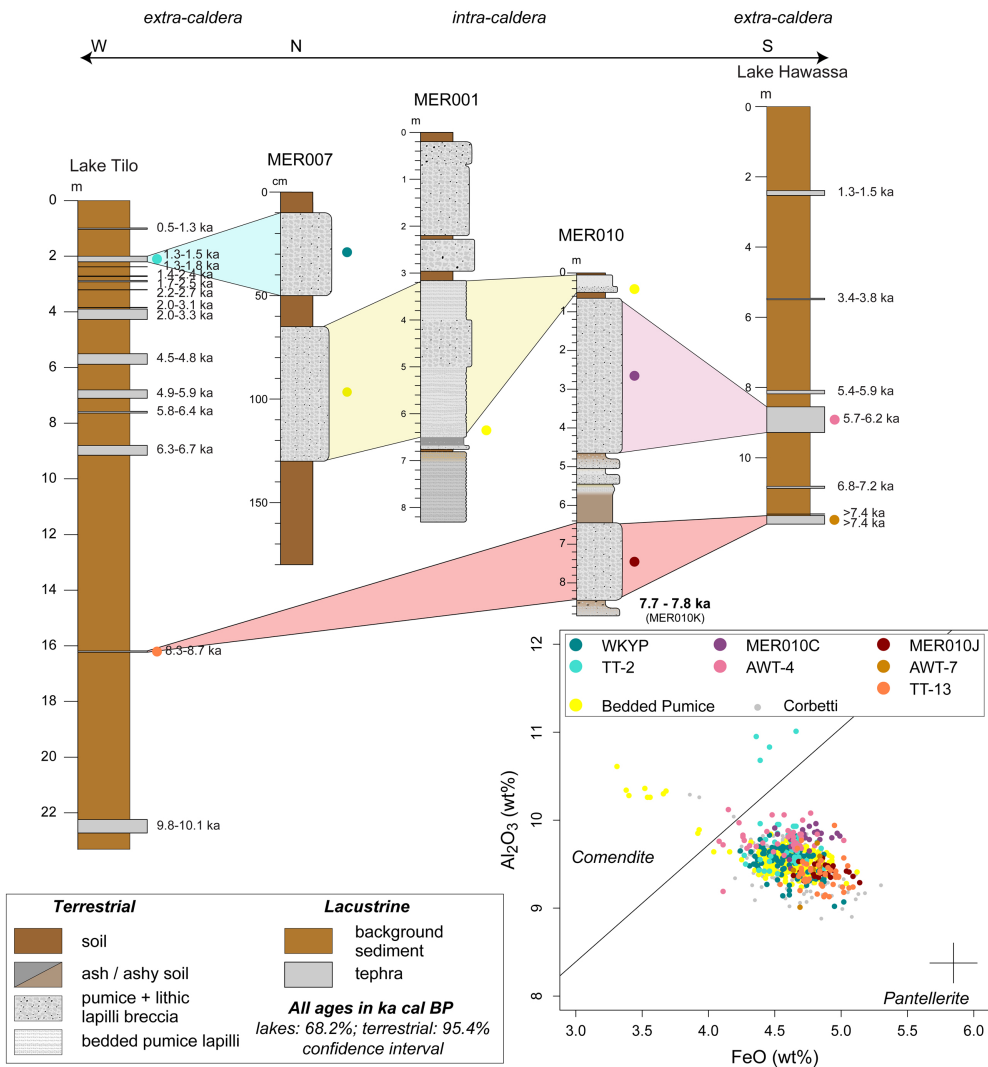
Figure 1

Figure 2

Figure 3

Corbetti

a. MER007
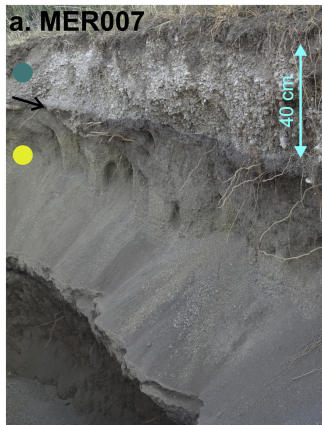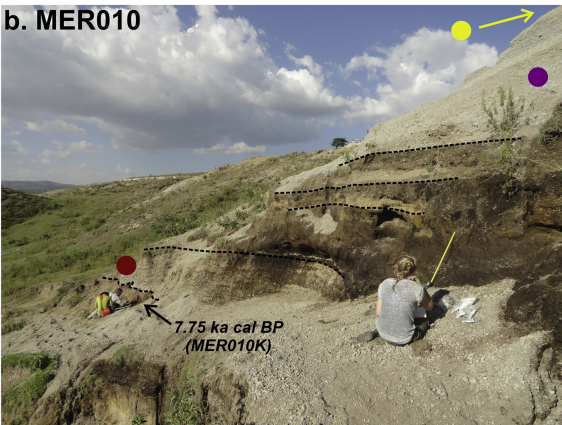
40 cm

b. MER010

7.75 ka cal BP
(MER010K)

Aluto

c. A01

d. MER046
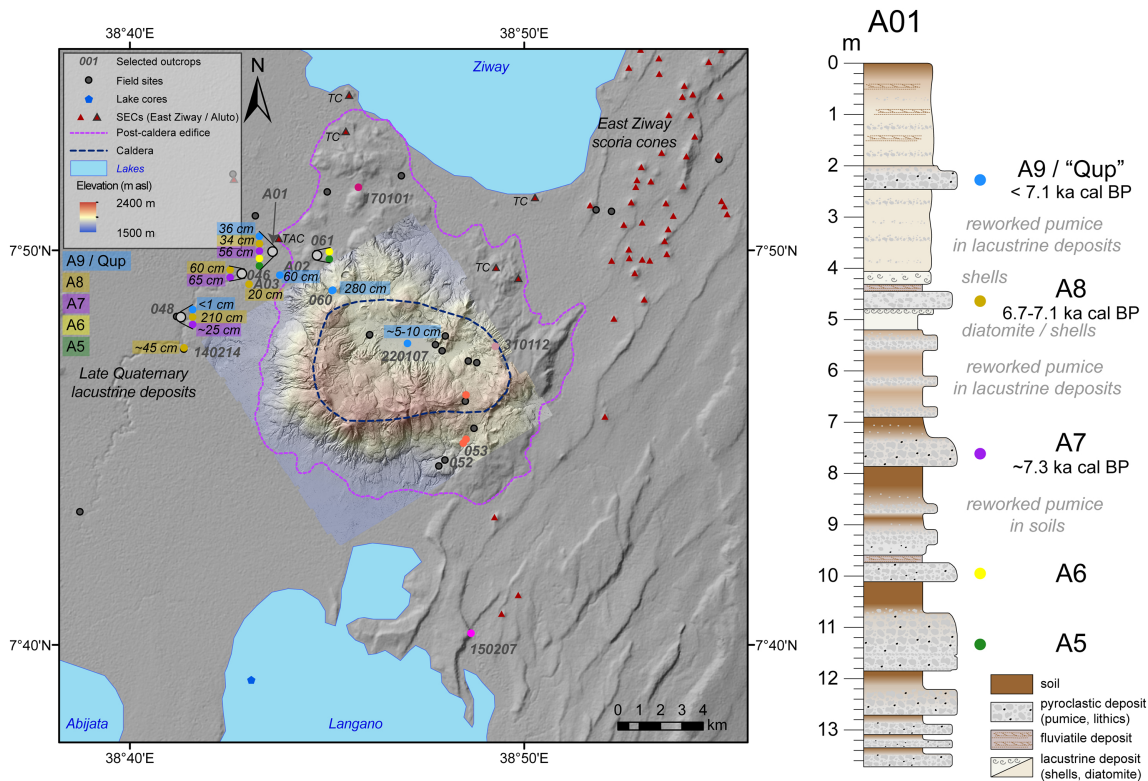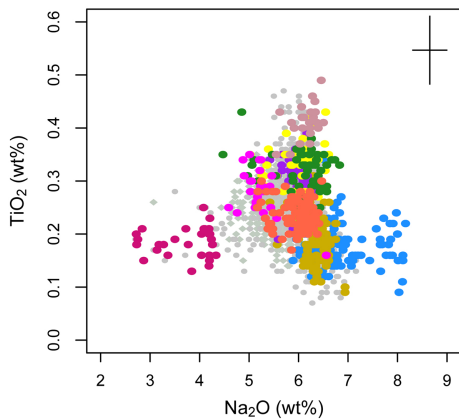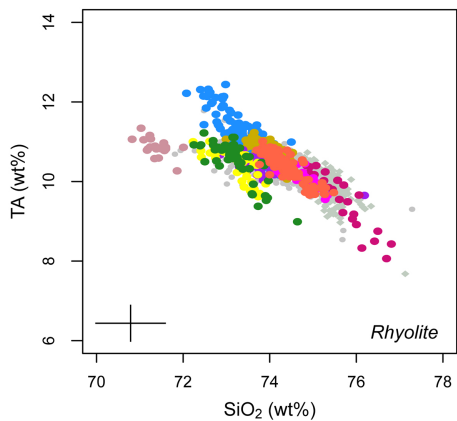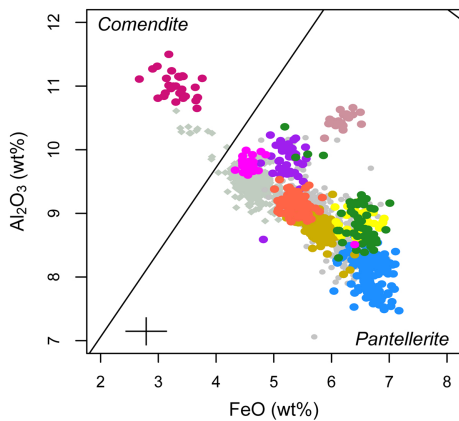
ash-rich top

clast-supported

Figure 4
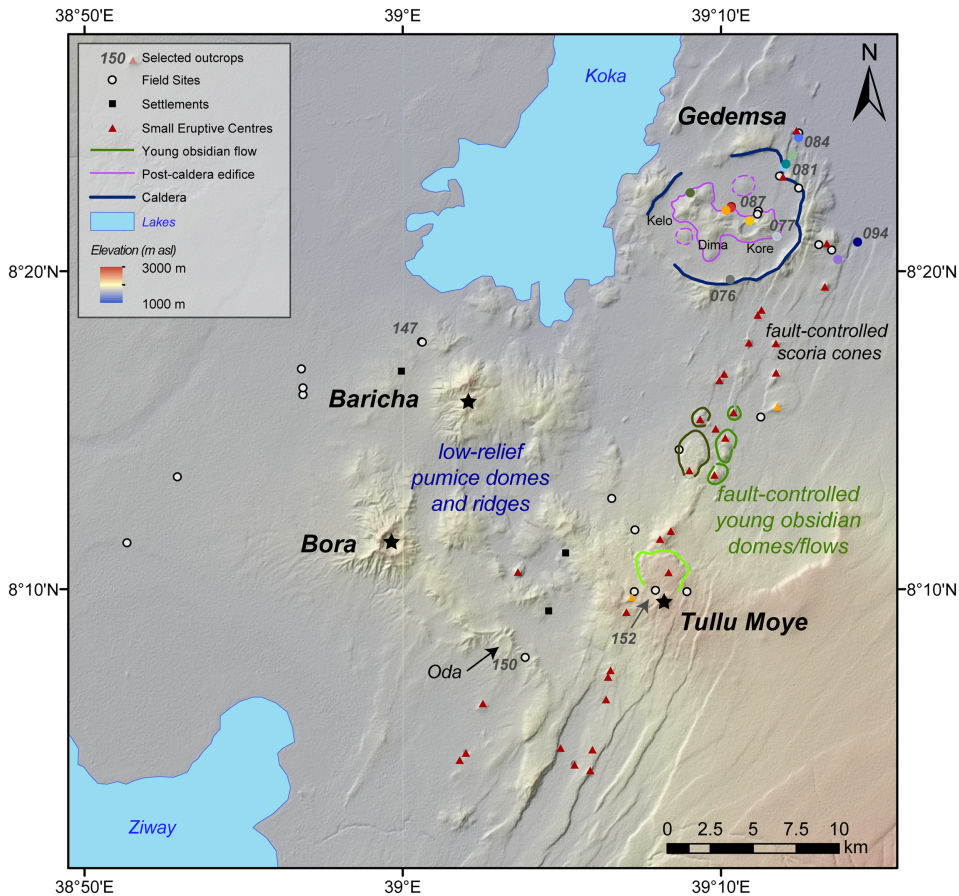
Figure 5
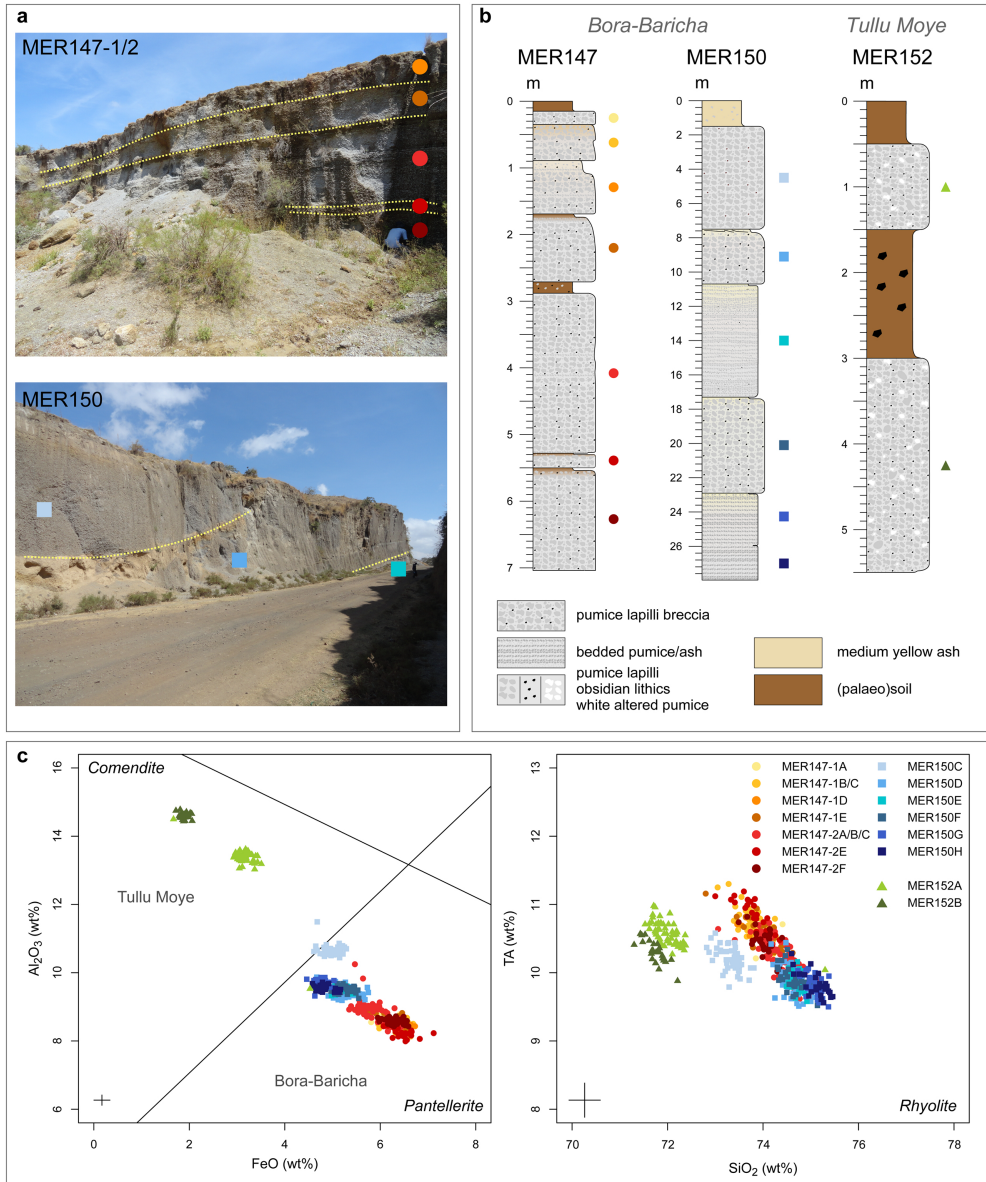
Figure 6

Figure 7

Figure 8
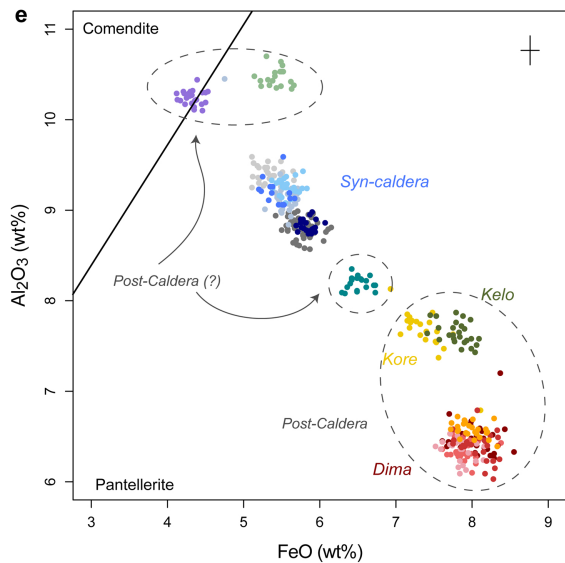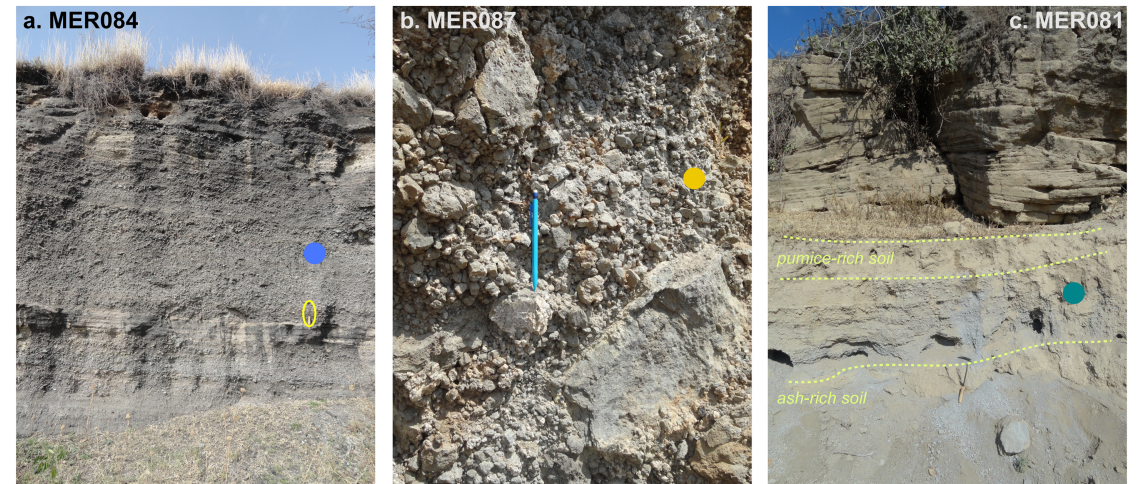
Figure 9

Figure 10

Figure 11

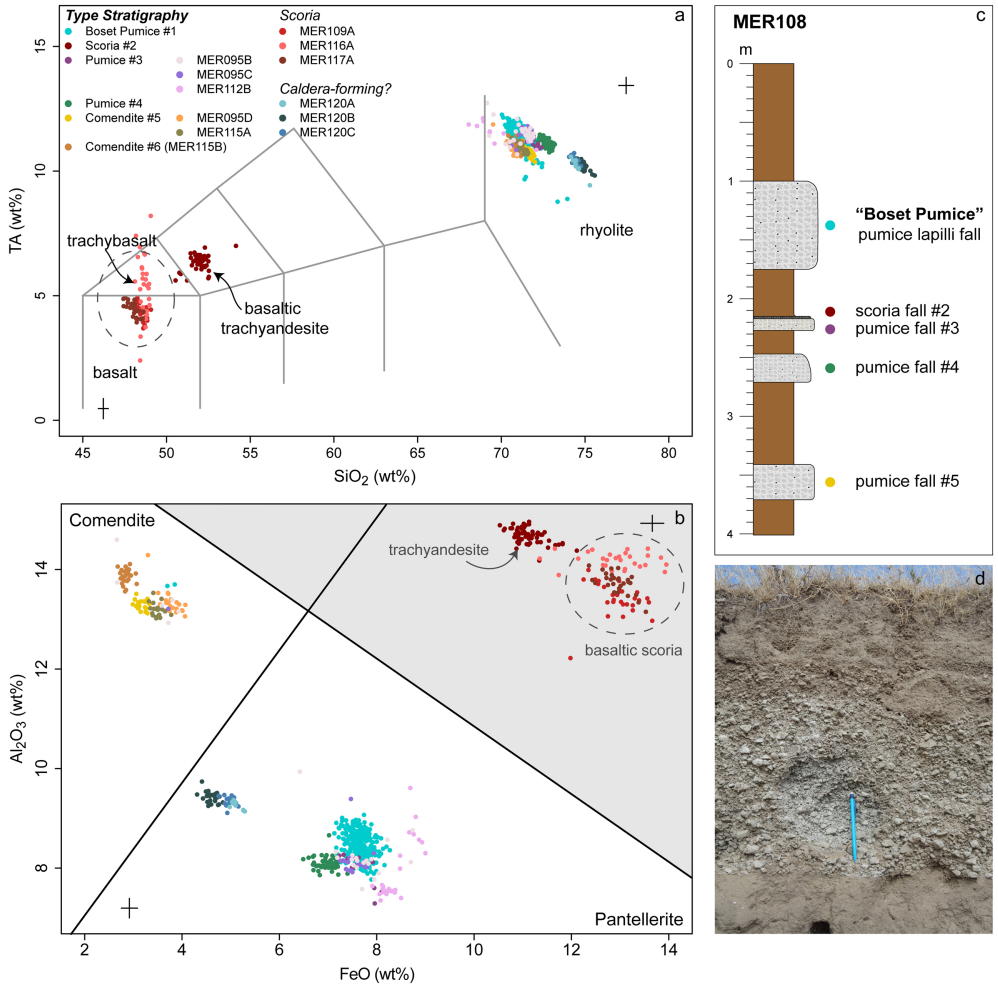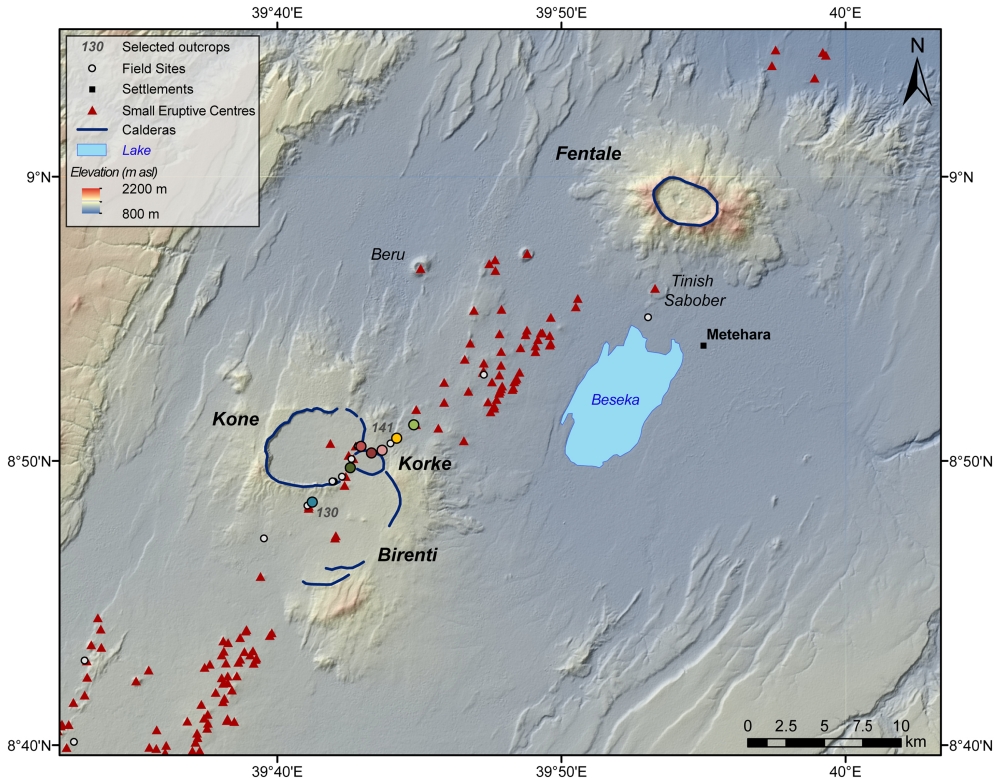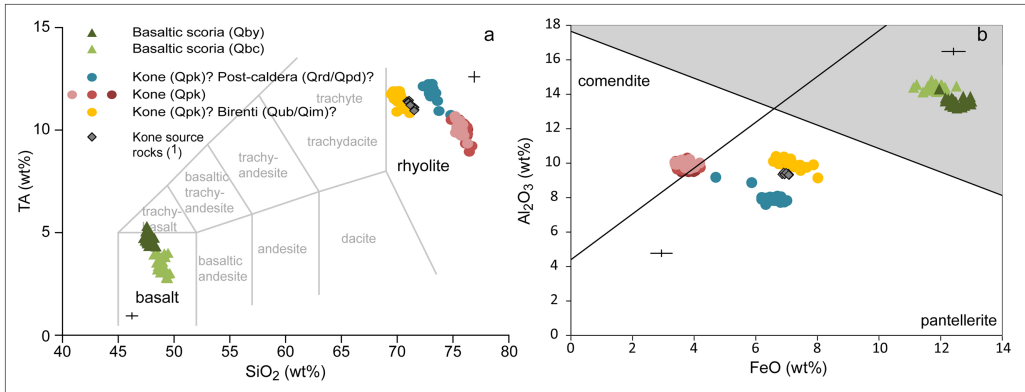Figure 12

Figure 13

Corbetti

a. MER001

b. MER013/14

Aluto

c. MER060

d. MER052

Figure 14